INORGANIC CHEMISTRY FRONTIERS

RESEARCH ARTICLE

View Article Online
View Journal

Check for updates

Cite this: DOI: 10.1039/d6qi00525j

A hybrid pyridine-thioether macrocycle to chelate theranostic copper and silver radioisotopes

Marianna Tosato, *[a,b] Fortuna Ponte,[c] Sara Franchi,[d] Nora V. May,[e] Mikael Jensen,[f] Helmut Mäcke,[g] Valerio Di Marco, [d] Laura Pigani, [h] Erika Ferrari, [h] Emilia Sicilia, [c] Mattia Asti[i] and Caterina F. Ramogida *[a,b]

Coinage radiometals such as $^{64/67}$Cu and $^{103/111}$Ag offer unique opportunities for cancer theranostics, providing matched diagnostic and therapeutic radionuclides within the same chemical family. However, their clinical translation is limited by the lack of robust chelators for $^{103/111}$Ag and by the redox-induced instability of $^{64/67}$Cu complexes. To address these chelation challenges, we developed DO2S2Py, a sulfur-containing cyclen (cy)-based macrocycle incorporating pyridine (py) donors, introduced to create a protected coordination environment for silver and copper ions. DO2S2Py rapidly forms highly thermodynamically stable and kinetically inert 1 : 1 metal-to-ligand complexes with both Cu^{2+} and Ag^{+}. Structural investigations reveal distinct yet strongly stabilized coordination environments for Cu^{2+} ($4N_{cy}2N_{py}$) and Ag^{+} ($4N_{cy}1N_{py}1S$ and $4N_{cy}2N_{py}$), underscoring the crucial contribution of the pyridine donors. Under highly diluted radiochemical conditions and mild labeling protocols, DO2S2Py efficiently binds ^{64}Cu and ^{111}Ag. The ^{64}Cu complex demonstrates exceptional stability in PBS and human serum (>95% intact complex after 24 h), while the ^{111}Ag analogue, though somewhat less stable (75% intact after 24 h), outperforms the current gold-standard chelator. These findings validate the incorporation of pyridine donors as an effective strategy toward unified chelation of theranostic coinage radiometals.

Received 19th March 2026,
Accepted 22nd April 2026

DOI: 10.1039/d6qi00525j

rsc.li/frontiers-inorganic

Open Access Article. Published on 23 April 2026. Downloaded on 6/3/2026 9:25:06 AM.
This article is licensed under a Creative Commons Attribution-NonCommercial 3.0 Unported Licence.

1. Introduction

The integration of radiometals into diagnostic and therapeutic radiopharmaceuticals has significantly advanced the field of precision medicine, enabling cancer imaging and targeted therapy at the molecular level. Within the broad spectrum of medically relevant radionuclides, group 11 radiometals, particularly copper and silver radioisotopes, have emerged as attractive candidates due to their favorable decay characteristics and suitability for diagnostic and therapeutic (*theranostic*) approaches.[1–4]

Among these, copper-64 (^{64}Cu, $t_{1/2}$ = 12.7 h) has a versatile emission profile that includes β^-, β^+ and electron capture decays and is highly suited for positron emission tomography (PET).[5] Complementarily, copper-67 (^{67}Cu, $t_{1/2}$ = 2.58 d) is a pure β^- emitter with accompanying low energy conversion and Auger electrons as well as γ rays that make it a candidate for therapy and single photon emission computed tomography (SPECT) imaging.[2,3,5–10] On the other hand, silver radioisotopes, including silver-103 (^{103}Ag, $t_{1/2}$ = 65.7 min) and silver-111 (^{111}Ag, $t_{1/2}$ = 7.45 d), have recently attracted interest for their theranostic potential despite being less explored.[1,5,11–15] These radioisotopes offer decay profiles suitable for β^- therapy and associated SPECT (^{111}Ag) or PET (^{103}Ag) imaging modalities.[1]

A major challenge in the development of group 11-based theranostic radiopharmaceuticals lies in designing chelators that can form thermodynamically stable and kinetically inert complexes with both copper and silver ions under physiological conditions.[16–21] Indeed, in the absence of such robust chelation, metal dissociation may occur *in vivo*, leading to uncontrolled redistribution of the radionuclide throughout the body. This can result in significant off-target toxicity, compromising patient safety and diminishing the diagnostic/therapeutic

[a]*Department of Chemistry, Simon Fraser University, V5A 4Y8 Burnaby, British Columbia, Canada. E-mail: marianna_tosato@sfu.ca, cfr@sfu.ca*
[b]*Life Sciences, TRIUMF, V6T 2A3 Vancouver, British Columbia, Canada*
[c]*Department of Chemistry and Chemical Technologies, University of Calabria, 87036 Cosenza, Italy*
[d]*Department of Chemical Sciences, University of Padova, 35131 Padova, Italy*
[e]*Centre for Structural Science, Research Centre for Natural Sciences, 1117 Budapest, Hungary*
[f]*The Hevesy Laboratory, Department of Health Technology, Technical University of Denmark, 4000 Roskilde, Denmark*
[g]*Department of Nuclear Medicine, University Hospital Freiburg, D-79106 Freiburg, Germany*
[h]*Department of Chemical and Geological Sciences, University of Modena and Reggio Emilia, 41125 Modena, Italy*
[i]*Radiopharmaceutical Chemistry Laboratory, Nuclear Medicine Unit, AUSL-IRCCS Reggio Emilia, 42122 Reggio Emilia, Italy*

Open Access Article. Published on 23 April 2026. Downloaded on 6/3/2026 9:25:06 AM. This article is licensed under a Creative Commons Attribution-NonCommercial 3.0 Unported Licence.

efficacy by preventing the radiation from reaching the tumor site. Developing a single ligand capable of effectively coordinating both copper and silver ions is also of strategic value, as it would enable the construction of chemically analogous radiopharmaceuticals that differ only in the choice of the radionuclide. Such a unified approach could streamline radiopharmaceutical development, simplify regulatory pathways, and offer clinicians a flexible toolkit for personalized nuclear medicine by switching between different diagnostic and therapeutic radioisotopes without altering the molecular architecture of the radiopharmaceutical.

Over the past decade, a variety of chelators, such as 1,4,7,10-tetraazacyclododecane-1,4,7,10-tetraacetic acid (DOTA), 1,4,8,11-tetraazacyclotetradecane-1,4,8,11-tetraacetic acid (TETA), and their cross-bridged analogues, have been developed to accommodate the borderline Lewis acid nature of $[^{64/67}Cu]Cu^{2+}$. Nonetheless, limitations such as *in vivo* transchelation, redox instability due to Cu^{2+} bioreduction to Cu^{+}, and slow radiolabeling kinetics have limited their broader clinical adoption.[9,22–32] More promising results have been achieved with 1,4,7-triazacyclononane-1,4,7-triacetic acid (NOTA) and its bifunctional derivative (NODAGA), as well as sarcophagine-based chelators (*e.g.*, DiamSar), which currently represent the gold standards for $[^{64/67}Cu]Cu^{2+}$ binding.[8] However, these chelators are poorly suited for Ag^{+}, which prefers softer donor atoms compared to Cu^{2+}.[33] Designing effective ligands for Ag^{+} remains especially demanding due to its high lability and strong tendency toward ligand exchange reactions. In fact, despite the growing interest in silver radioisotopes for theranostic applications, the coordination (radio) chemistry of Ag^{+} remains largely unexplored, highlighting the need for further systematic studies.[34–37]

In response to these challenges, in recent years, our research group has focused on developing chelators for soft (radio)metals.[38–46] In particular, we previously synthesized and characterized a library of sulfur-rich macrocyclic ligands tailored to the coordination preferences of group 11 metals (Fig. 1 and Fig. S1).[38–44,47] These ligands exhibited high affinity for both $Cu^{2+/+}$ and Ag^{+}, even under highly dilute radiochemical conditions. Among them, 1,7-bis[2-(methylsulfanyl)ethyl]-1,4,7,10-tetraazacyclododecane-4,10-diacetic acid (DO2A2S) emerged as the top-performing candidate for copper radioisotopes, while 1,4,7,10-tetrakis[2-(methylsulfanyl)ethyl]-1,4,7,10-tetraazacyclododecane (DO4S) showed the best performance for silver radionuclides.[41,43] However, the $[^{111}Ag][Ag(DO4S)]^{+}$ complex demonstrated limited stability in human serum, undergoing a noticeable degradation within a few hours.[43] While this may still be acceptable for proof-of-concept preclinical investigations with short-lived Ag radioisotopes (*e.g.*, ^{103}Ag), it highlights the need for improved chelation strategies for this metal ion, especially for longer imaging windows or therapeutic use.

To overcome these limitations and develop a single versatile platform for the chelation of group 11 radiometals, in the present study we designed a novel octadentate macrocycle, namely 1,7-bis[2-(methylsulfanyl)ethyl]-4,10-bis[(pyridin-2-yl)methyl]-1,4,7,10-tetraazacyclododecane (DO2S2Py) (Fig. 1). The choice of a cyclen (cy) backbone was driven by our previous comparative studies, in which cyclen-based ligands outperformed those containing different macrocyclic cores (Fig. 1 and Fig. S1) in terms of stability and coordination efficiency with both $Cu^{2+/+}$ and Ag^{+}.[38–40,42,43] We retained the two opposite sulfur-containing pendant arms, as they had previously shown a fundamental role in the metal coordination.[38–40,42,43] To enhance complex robustness, we inserted two pyridine (py) moieties in the trans (1,7-*N*,*N*″-) positions. These moieties were selected for their known affinity for copper and silver, and their steric bulkiness, which we hypothesized would help to enforce a more spatially shielded coordination environment.[48–51] This conformational constraint is expected to benefit the kinetic stabilization of the metal center, in particular Ag^{+} (the more labile metal ion), by reducing the susceptibility of the complex to dissociation or transchelation by endogenous biomolecules.

In this work, we report the synthesis and a comprehensive theoretical and experimental evaluation of DO2S2Py as a chelator for both copper and silver radioisotopes for nuclear medicine applications. We investigated its solution behavior, deter-

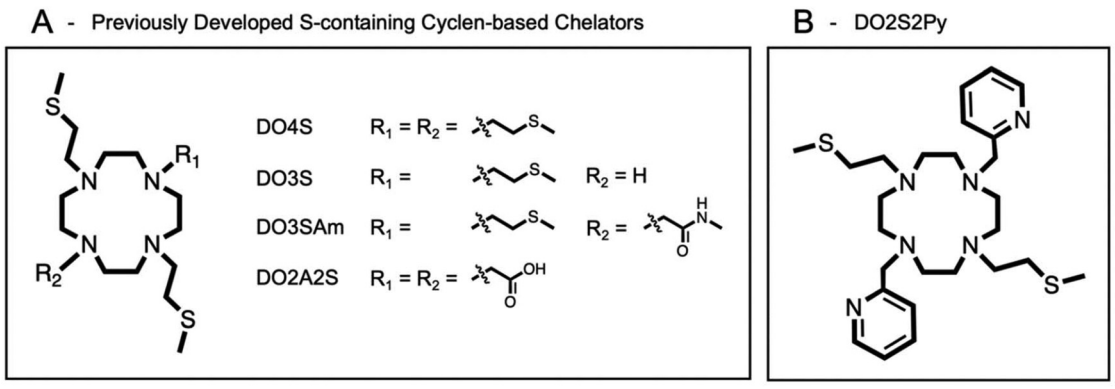

Fig. 1 Chemical structures of (A) previously developed sulfur-containing cyclen-based chelators for copper and silver radioisotopes and (B) the chelator investigated in this work; DO2S2Py is shown in its neutral, completely deprotonated, form.

 This journal is © the Partner Organisations 2026

Open Access Article. Published on 23 April 2026. Downloaded on 6/3/2026 9:25:06 AM. This article is licensed under a Creative Commons Attribution-NonCommercial 3.0 Unported Licence.

mined the thermodynamic stability constants, studied the complexation and decomplexation kinetics, and elucidated the solution structures of its Cu^{2+} and Ag^{+} complexes. The ability of DO2S2Py to bind $[^{64}Cu]Cu^{2+}$ and $[^{111}Ag]Ag^{+}$ under extremely diluted radiochemical conditions was also assessed and complemented with the evaluation of the *in vitro* stability of the corresponding radioactive complexes in biological environment, a pillar requirement for further *in vivo* applications.

2. Results and discussion

2.1. Synthesis of DO2S2Py

DO2S2Py was obtained according to the synthetic pathway illustrated in Scheme 1. The synthesis began with the selective protection of two opposite nitrogen atoms (N_1, N_7) of the cyclen ring (**1**) using *N*-(*tert*-butyloxycarbonyloxy)succinimide (Boc-OSu) in dry methanol, affording 1,7-bis(*tert*-butyloxycarbonyl)-1,4,7,10-tetraazacyclododecane (**2**, di-Boc-cyclen). This protection strategy was introduced to enable regioselective functionalization of the macrocycle as direct alkylation would otherwise lead to non-selective mixtures of substitution patterns. Boc protection of two nitrogen atoms allows a controlled trans-functionalization pattern in the subsequent steps.

In the second step, di-Boc-cyclen was reacted with 2-chloroethylmethyl sulfide in acetonitrile in the presence of K_2CO_3 to yield 1,7-bis(*tert*-butyloxycarbonyl)-4,10-bis(2-(methylsulfanyl)ethyl)-1,4,7,10-tetraazacyclododecane (**3**, di-Boc-DO2S). Subsequent acidic deprotection using trifluoracetic acid (TFA) in dichloromethane afforded 1,7-bis(2-(methylsulfanyl)ethyl)-1,4,7,10-tetraazacyclododecane as a TFA salt (**4**, DO2S), which was then alkylated with 2-(bromomethyl)pyridine hydrobromide in acetonitrile and in presence of K_2CO_3 to produce DO2S2Py (**5**). All the intermediates and DO2S2Py were fully characterized by Nuclear Magnetic Resonance (NMR – ^{1}H NMR, $^{13}C\{^{1}H\}$ NMR, ^{1}H–^{1}H COSY, and ^{1}H–^{13}C HSQC), and high-resolution mass spectrometry (HR-MS). The corresponding spectra are reported in Fig. S2–S15. The overall multistep synthesis allowed to provide the pure chelator DO2S2Py, although in low yield (8%).

2.2. Acid–base properties of DO2S2Py

Before investigating the coordination behavior of DO2S2Py toward Cu^{2+} and Ag^{+}, a comprehensive characterization of its acid–base properties in aqueous solution was carried out. Specifically, the acidity constants (pK_a) of the new chelator were determined by pH-potentiometry and pH-dependent ^{1}H NMR and UV-Vis spectroscopic titrations. Multiple complementary techniques were employed to provide independent and mutually consistent datasets. This characterization step is essential, as the protonation state of the ligand directly impacts its metal-binding ability due to the intrinsically competitive nature of protonation and metal coordination equilibria.

The ^{1}H NMR spectra of DO2S2Py as a function of pH are shown in Fig. 2, along with signal assignments. The methyl protons (H_1) of the thioether arms (SCH_3) of DO2S2Py remain almost unaffected across the investigated pH range, consistently appearing as a singlet at ~2 ppm. This behavior is attributed to their positioning far from the proton binding sites, making them essentially insensitive to the protonation state of the molecule. In contrast, all the other proton signals display a clear pH dependence, consistent with their proximity to protonable sites. At acidic pH, the methylene protons of the sulfur-containing sidechains (SCH_2 and NCH_2, H_2 and H_3) appear as two distinct broad singlets at 2.85 and 3.35 ppm, respectively. As the pH increases, these signals shift upfield and coalesce into a single resonance at 2.50 ppm at pH > 12. A similar trend is also observed for the NCH_2 protons (H_4) of the macrocyclic ring (*i.e.* they resonate as two separate singlets at 3.60 and 3.22 ppm at pH 2, and merge into one signal at 2.95 ppm above pH 12). The CH_2 protons bridging the pyridine rings and the macrocycle (H_5) resonate as a singlet throughout the titration but exhibit a continuous variation in chemical shift with increasing pH. The aromatic region also displays pronounced pH-dependent changes: the pyridine protons experience progressive upfield shifts upon deprotonation while the *meta* protons (H_6 and H_8) relative to the aromatic N coalesce into a single resonance below pH 7. The *ortho* (H_9) and *para* (H_7) protons remain distinct across the entire pH range. The pH-dependent chemical shift trends were fitted to derive the pK_a values, reported in Table 1. The obtained data were corroborated by pH-potentiometric titrations (Table 1).

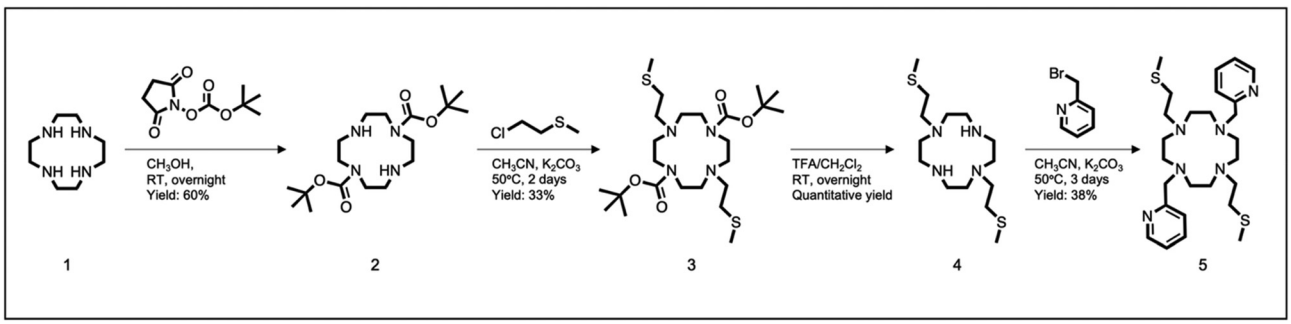

Scheme 1 Synthesis of DO2S2Py.

Open Access Article. Published on 23 April 2026. Downloaded on 6/3/2026 9:25:06 AM.
This article is licensed under a Creative Commons Attribution-NonCommercial 3.0 Unported Licence.

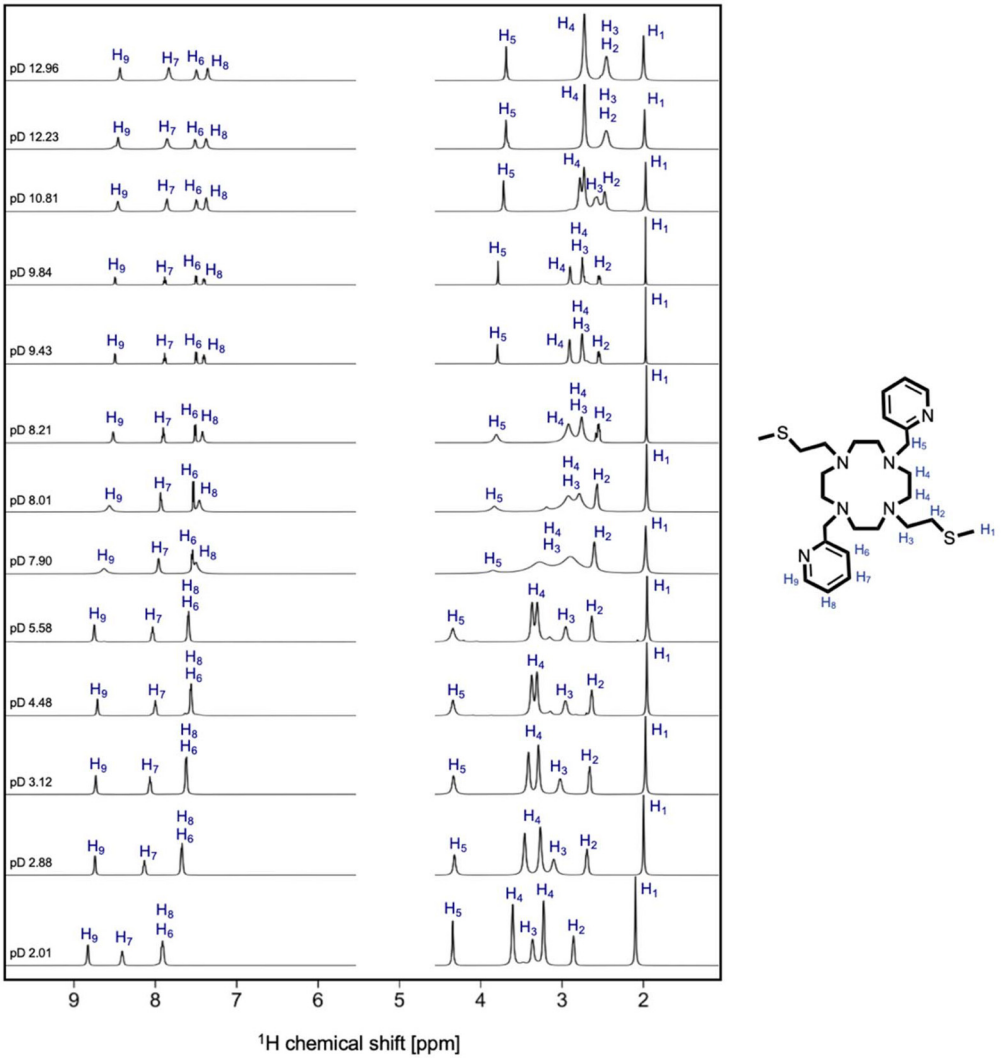

Fig. 2 Representative ^{1}H NMR spectra of DO2S2Py at different pH (400 MHz, D_2O, T = 25 °C, I = 0.15 M NaCl or 0.15 M $NaNO_3$, $C_{DO2S2Py}$ = 1 × 10^{-3} M). Note: no effect of different ionic strength was observed.

Table 1 Acidity constants (pK_a) of DO2S2Py and overall stability constants (logβ) of its Cu^{2+} and Ag^+ complexes (I = 0.1 M NaCl (Cu^{2+})/$NaNO_3$ (Ag^+), T = 25 °C) obtained with the different techniques

Equilibria[a]	^{1}H NMR	Potentiometry pK_a	UV-Vis
$HL^+ \rightleftharpoons L + H^+$	10.76 ± 0.03	10.8 ± 0.1	—
$H_2L^{2+} \rightleftharpoons HL^+ + H^+$	7.75 ± 0.09	7.82 ± 0.05	7.78 ± 0.1
$H_3L^{3+} \rightleftharpoons H_2L^{2+} + H^+$	3.10 ± 0.06	3.19 ± 0.05	3.33 ± 0.02
$H_4L^{4+} \rightleftharpoons H_3L^{3+} + H^+$	2.6 ± 0.1	—	2.53 ± 0.02
Equilibria[a]		logβ	
$Cu^{2+} + L \rightleftharpoons [CuL]^{2+}$	—	—	23.62 ± 0.07
$Ag^+ + L \rightleftharpoons [AgL]^+$	16.94 ± 0.08	16.83 ± 0.04	—
$Ag^+ + HL \rightleftharpoons [AgHL]^{2+}$	20.64 ± 0.05	20.6 ± 0.1	—
$Ag^+ + L + H_2O \rightleftharpoons [AgL(OH)] + H^+$	6.65 ± 0.09	6.6 ± 0.1	—

[a] L represents the completely deprotonated form of DO2S2Py as shown in Fig. 1. The reported uncertainty was obtained by the fitting procedure and represents one standard deviation unit.

This journal is © the Partner Organisations 2026

Open Access Article. Published on 23 April 2026. Downloaded on 6/3/2026 9:25:06 AM. This article is licensed under a Creative Commons Attribution-NonCommercial 3.0 Unported Licence.

The corresponding species distribution diagram is presented in Fig. S16. These results indicate that a mixture of bi- and monoprotonated species (H_2L^{2+} and HL^{+}) exist under physiological pH conditions.

DO2S2Py is formally a hexaprotic molecule, containing four tertiary amines within the macrocyclic ring and two pyridine nitrogen atoms. However, only four pK_a values could be determined under our experimental conditions. The last two (p$K_{a,5}$ and p$K_{a,6}$) are attributed to the deprotonation of the two macrocyclic nitrogen atoms located opposite each other (Table 1). This assignment is supported by previous studies on cyclen-based ligands, which show preferential protonation at opposite sites to minimize electrostatic repulsion between adjacent protonated centers.[47] The intermediate two pK_a (p$K_{a,3}$ and p$K_{a,4}$) are ascribed to the deprotonation of the pyridine nitrogen atoms (Table 1). The first two protonation steps (p$K_{a,1}$ and p$K_{a,2}$), corresponding to the remaining tertiary amines of the cyclen ring, were not detected, likely due to their very low values (pK_a < 1). These highly protonated species are typically unstable and only appreciably formed at extremely acidic pH (pH < 1), making their detection challenging. This behavior is well-documented in the literature and is a characteristic of cyclen-based macrocycles.[47,52]

The pK_a values associated with the macrocyclic amine groups of DO2S2Py closely resemble those previously reported for sulfur-containing analogues such as DO4S, as well as for pyridine-functionalized derivatives including cyclen-1Py, cyclen-2Py, and cyclen-4Py (Table S1).[47,50,51] Similarly, the pK_a values attributed to the pyridine moieties of DO2S2Py are in good agreement with those of related ligands bearing only pyridine substituents (Table S1).[50,51] This indicates that the presence of the sulfanyl side chains does not significantly perturb the protonation behavior of the pyridine nitrogen atoms, suggesting minimal electronic/steric influence on their basicity.

The protonation constants determined by ^{1}H NMR spectroscopy were further corroborated through pH-dependent UV-Vis spectrophotometric titrations. Representative pH-dependent electronic spectra of DO2S2Py are shown in Fig. S17. The UV-Vis spectrum of DO2S2Py exhibits electronic transitions originating from both the aliphatic sulfur-containing macrocyclic core, which gives rise to absorption bands below 250 nm, and the pyridine rings, characterized by a distinct absorption maximum centered at 262 nm. The latter band closely resembles that observed for the monopyridine-functionalized cyclen analogue (cyclen-Py), suggesting that it can be attributed to the π–π* transitions of the pyridine moieties.[50] Systematic pH-dependent variations in the electronic absorption spectra enabled the determination of the acidity constants of the ligand (p$K_{a,2}$, p$K_{a,3}$, and p$K_{a,4}$), which are summarized in Table 1. Notably, these values are in excellent agreement with those obtained with other techniques.

2.3. Kinetics of DO2S2Py complexes formation

Before evaluating the thermodynamic stability of the Ag^+ and Cu^{2+} complexes of DO2S2Py, the formation kinetics of these species were qualitatively investigated.

2.3.1. Cu^{2+}-DO2S2Py. In the case of Cu^{2+}, kinetic studies were performed by UV-Vis spectroscopy at different pH values (pH 2, 4.5, and 7). Representative spectra are reported in Fig. S18. In all cases, the addition of Cu^{2+} to the ligand solution induced an immediate change in the electronic spectra of DO2S2Py. Notably, an enhanced absorbance at wavelengths beyond the absorption maximum (>270 nm), along with a broad band centered around 677 nm, was observed compared to the free ligand (Fig. S18 and S19). No significant spectral changes were detected over time. These data provide clear evidence of complex formation under the investigated pH conditions. Moreover, these findings indicate that DO2S2Py coordinates Cu^{2+} instantaneously across the investigated pH range, regardless of the protonation state of the ligand. This behavior is in contrast with previous observations for structurally analogous sulfur-containing chelators lacking pyridine moieties (DO4S, DO3S and DO3SAm, Fig. 1), where markedly slower complexation kinetics were observed at progressively more acidic pH due to increased electrostatic repulsion between the dicationic Cu^{2+} ion and highly protonated ligand species.[38] For example, in the case of DO4S, complexation at pH 2 required up to 10 days to reach equilibrium (Table S2).[38] The significantly enhanced formation kinetics observed for DO2S2Py highlight the key role played by the pyridine groups in accelerating the complexation event.

2.3.2. Ag^+-DO2S2Py. A similar behavior was observed for Ag^+: the addition of the metal ion to a solution of DO2S2Py induced immediate and distinct changes in the ^{1}H NMR spectra compared to the free ligand (Fig. S20), consistent with the rapid formation of Ag^+-DO2S2Py complexes. These spectral modifications occurred without any detectable time evolution, indicating that complexation reaches equilibrium faster than the timescale of experimental acquisition. Notably, such fast complexation kinetics with Ag^+ are consistent with previous observations for related S-rich chelators in the absence of pyridine units, suggesting that silver coordination is inherently more rapid and less sensitive to the nature of the auxiliary donor groups compared to Cu^{2+}.[42,43]

2.4. Thermodynamic stability of DO2S2Py complexes

The stability constants (logβ) of Cu^{2+}-DO2S2Py and Ag^+-DO2S2Py complexes were determined using UV-Vis (Cu^{2+}), ^{1}H NMR (Ag^+) spectroscopic titrations as well as potentiometry (Cu^{2+} and Ag^+).

2.4.1. Cu^{2+}-DO2S2Py. Representative electronic spectra of Cu^{2+}-DO2S2Py recorded at various pH values and the corresponding pH-dependent absorbance profile at a selected wavelength are presented in Fig. S21.

No significant spectral changes were observed in the pH range 3–12, indicating that the speciation remains constant across this range and that a single Cu^{2+}-containing species predominates. In contrast, at pH < 3, a marked decrease in absorbance was noted, and the spectral features increasingly resembled those of the free ligand (compare Fig. 2 with Fig. S21). This behavior is consistent with proton-induced dissociation of the complex and the release of the uncoordinated

Open Access Article. Published on 23 April 2026. Downloaded on 6/3/2026 9:25:06 AM. This article is licensed under a Creative Commons Attribution-NonCommercial 3.0 Unported Licence.

ligand occurring at highly acidic media (pH < 2). These spectroscopic data were fitted using a suitable equilibrium model, yielding the stability constant reported in Table 1. According to the derived speciation, DO2S2Py forms a single mononuclear complex with Cu^{2+}, namely $[CuL]^{2+}$. The stoichiometry of the complex was further confirmed by pH-potentiometry and mass spectrometry (Fig. S22). The latter revealed a single peak corresponding to the 1 : 1 metal-to-ligand species, with no evidence of polynuclear aggregates. The corresponding speciation diagram is presented in Fig. 3.

Interestingly, compared to previously developed sulfur-containing analogues (*e.g.*, DO4S), the Cu^{2+} complexation behavior of DO2S2Py is identical in terms of speciation: in all cases, only the fully deprotonated mononuclear species is formed.[38] This suggests that the presence of the pyridine moiety does not alter the speciation profile. The formation of protonated species appears disfavored, likely due to the neutral nature of the ligand, which would lead to highly charged complexes ($[CuHL]^{3+}$, $[CuH_2L]^{4+}$ *etc.*). The speciation model is also consistent with that of Cu^{2+}-cyclen-1Py but differs from that of Cu^{2+}-cyclen-2Py, where additional species such as the monoprotonated complex ($[CuHL]^{3+}$) and a hydroxo-containing complex ($[CuL(OH)]^{+}$) were observed (however, in this case, a different supporting electrolyte was used, *i.e.* NMe_4NO_3).[50,51]

2.4.2. Ag^+-DO2S2Py. The ^{1}H NMR spectra of Ag^+-DO2S2Py recorded at different pH values are shown in Fig. S23 (the signal attribution was performed with the aid of 2D homo- and hetero-correlated NMR experiments; representative 2D spectra are reported in Fig. S24 and S25). These spectra differ markedly from that of the free ligand (Fig. 2), indicating successful metal coordination.

At pH values above 11, the ^{1}H NMR spectra are invariant, suggesting the predominance of a single species. Similarly, in the pH range 5–8, the ^{1}H NMR spectra remain unchanged, implying the existence of a second complex. Below pH 4, additional spectral changes are observed, consistently with the presence of other species. The pronounced pH sensitivity of the spectra supports the presence of multiple, pH-dependent complexes differing in their protonation state, as also indicated by pH-potentiometry. The obtained ^{1}H NMR and pH-potentiometric data were fitted to a suitable equilibrium model, from which the stability constants of the complexes were derived (Table 1). According to the proposed speciation model, DO2S2Py forms exclusively 1 : 1 metal-to-ligand complexes, namely $[AgHL]^{2+}$, $[AgL]^{+}$ and [AgL(OH)]. The corresponding species distribution diagram is reported in Fig. 3.

As with Cu^{2+}, the speciation model determined for Ag^+-DO2S2Py closely resembles those previously reported for analogous sulfur-containing chelators.[42,43] The only notable difference is the detection of a hydroxo complex with this ligand, which was not observed for other cyclen-based chelators. The differences observed between Ag^+ and Cu^{2+} also reflect previous findings, where the lower charge of Ag^+ had shown to favor the formation of more protonated species.[38,42]

2.4.3. Stability comparisons. To enable a meaningful comparison of complex stability across systems involving ligands with different basicity, metal ions with distinct hydrolysis behavior, or complexes with varying stoichiometries, it is essential to calculate pM values. Defined as $pM = -\log [M]_{free}$, where $[M]_{free}$ is the concentration of unbound metal ion at equilibrium, this parameter offers a standardized and practical metric of the effective metal-binding affinity of a ligand under biologically relevant conditions.[53] Indeed, unlike stability constants (log*K*), pM values account for proton competition and metal hydrolysis, enabling direct and quantitative comparisons between different systems.

The high values observed for the pCu^{2+} and pAg^+ of DO2S2Py indicate that the ligand exhibits strong affinity toward both metal ions (Fig. 4).

When benchmarked against the sulfur-containing chelators previously developed (*e.g.*, DO4S and DO2A2S), as well as established ligands like NOTA and DOTA, DO2S2Py exhibits exceptional affinity for Cu^{2+} (Fig. 4).[38] In particular, its pCu^{2+} value (pCu^{2+} = 20) exceeds that of DO2A2S (pCu^{2+} = 19.4), previously identified as our best-performing S-rich Cu^{2+} chelator,

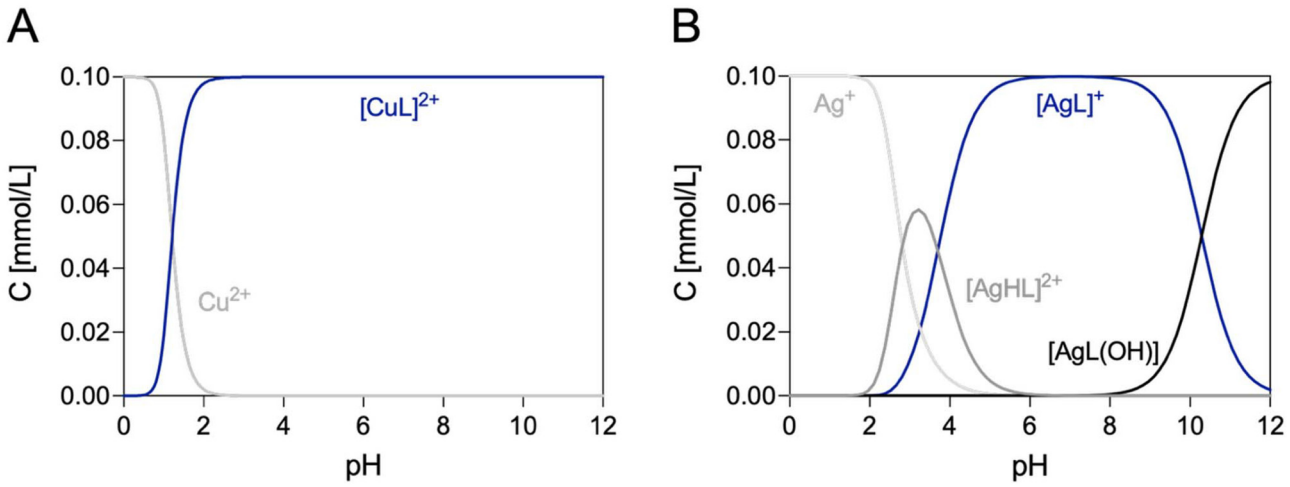

Fig. 3 Distribution diagrams of (A) Cu^{2+}-DO2S2Py and (B) Ag^+-DO2S2Py ($C_{DO2S2Py} = 1 \times 10^{-4}$ M, $C_M = 1 \times 10^{-4}$ M, M = Cu^{2+} or Ag^+).

 This journal is © the Partner Organisations 2026

Open Access Article. Published on 23 April 2026. Downloaded on 6/3/2026 9:25:06 AM.
This article is licensed under a Creative Commons Attribution-NonCommercial 3.0 Unported Licence.

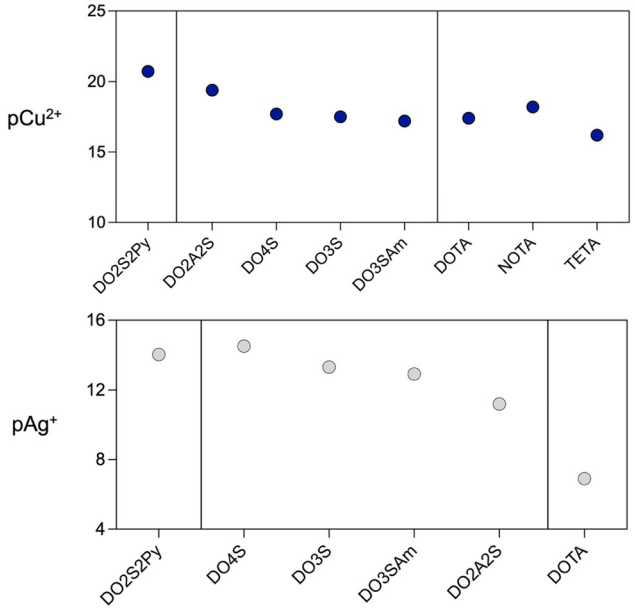

Fig. 4 Comparison of pCu^{2+} and pAg^{+} values of the Cu^{2+} and Ag^{+} complexes formed with DO2S2Py and various state-of-the-art chelators. pCu^{2+} and pAg^{+} values were calculated at pH 7.4, $C_{DO2S2Py} = 1 \times 10^{-5}$ M and $C_M = 1 \times 10^{-6}$ M (M = Cu^{2+} or Ag^{+}).

as well as those of NOTA (pCu^{2+} = 18.2), DOTA (pCu^{2+} = 17.4) and TETA (pCu^{2+} = 16.2).[38] Notably, compared to other cyclen-based pyridine-containing ligands (*e.g.*, cyclen-2Py and cyclen-1Py), DO2S2Py consistently forms more stable Cu^{2+} complexes (Fig. S26).[50,51] This enhancement in stability suggests that the simultaneous presence of soft (S) and borderline (N) donor atoms allows us to fine-tune the ligand's coordination environment improving metal binding. Regarding Ag^{+}, the complex formed with DO2S2Py exhibits thermodynamic stability nearly identical (pAg^{+} = 14) to Ag^{+}-DO4S (pAg^{+} = 14.5), the current benchmark chelator for silver radioisotopes (Fig. 4).[42] These results underscore the versatility of DO2S2Py as a chelator capable of effectively coordinating these metal ions despite their different coordination preferences, highlighting its potential for radiopharmaceutical applications.

2.5. Structure of DO2S2Py complexes in aqueous environment

The coordination geometries of Cu^{2+}-DO2S2Py and Ag^{+}-DO2S2Py in aqueous environment were investigated using a multifaceted theoretical and experimental approach that combined NMR (Ag^{+}), Electron Paramagnetic Resonance (EPR, Cu^{2+}) and UV-Vis (Cu^{2+}) spectroscopies with Density Functional Theory (DFT) calculations (Cu^{2+} and Ag^{+}).

2.5.1. Cu^{2+}-DO2S2Py. Frozen solution EPR spectra of Cu^{2+}-DO2S2Py mixtures at varying pH values are presented in Fig. 5. These data indicate that, across the investigated pH range (2–10), only a single predominant complex exists (*i.e.* $[CuL]^{2+}$), in addition to the Cu^{2+}-aqua complex, supporting the conclusions drawn from UV-Vis spectroscopy and potentiometry.

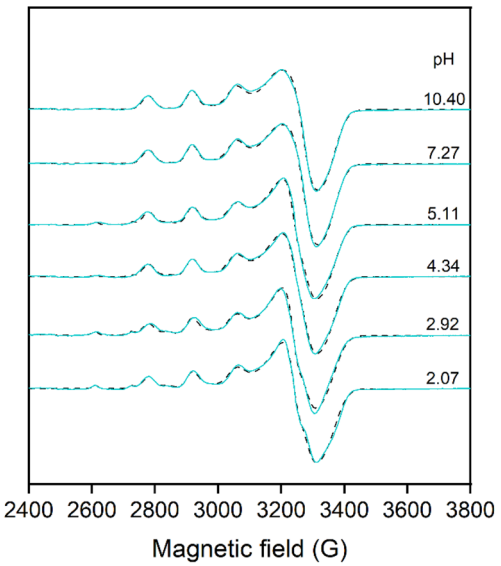

Fig. 5 Measured (black) and simulated (blue) frozen EPR spectra of Cu^{2+}-DO2S2Py at different pH.

No protonated, mixed hydroxo-complexes, or other geometrical isomers could be observed by EPR.

The EPR spectrum of $[Cu(DO2S2Py)]^{2+}$ in frozen solution is notably broad (Fig. 5) and could be described with parameters $g_\perp$ = 2.067, $g_\parallel$ = 2.248, and $A_\parallel = 144 \times 10^{-4}$ cm^{-1}. Due to the broad perpendicular line, approximate axial *g*- and *A*-tensors could be simulated (Table 2), with considerable uncertainty in the perpendicular components. This pronounced broadening is likely the result of rhombic distortion in the coordination geometry, indicating a deviation from axial symmetry.

In Table S3, the EPR parameters of several relevant Cu^{2+} macrocyclic complexes are compared with the values obtained in the present study.[38,51] Based on this comparison, 4N and 4NS coordination modes can be excluded, as these typically exhibit significantly smaller $g_\parallel$ values and larger $A_\parallel$ values than those observed for $[Cu(DO2S2Py)]^{2+}$. Instead, the parameters are closer to those reported for DO2A2S, in which two carboxylate side chains and two ring nitrogens occupy the equatorial plane, while the remaining two macrocyclic nitrogens are located farther from the metal center in axial positions.[38]

A similar coordination mode can be envisaged for Cu^{2+}-DO2S2Py if the pyridine nitrogens coordinate in place of the

Table 2 EPR parameters obtained by the simulation of EPR spectra of $[Cu(DO2S2Py)]^{2+}$ in frozen solution

Anisotropic parameters[a]						
g_x	g_y	g_z	$A_x/10^{-4}$ cm^{-1}	$A_y/10^{-4}$ cm^{-1}	$A_z/10^{-4}$ cm^{-1}	$g_{0,calc}$[b]
2.067	2.067	2.248	12	12	144	2.127

[a] The experimental errors were ± 0.002 for g_x and g_y and ± 0.001 for g_z, ± 2×10^{-4} cm^{-1} for A_x and A_y and ± 1×10^{-4} cm^{-1} for A_z. [b] Calculated with the equation $g_{0,calc} = (g_x + g_y + g_z)/3$.

Open Access Article. Published on 23 April 2026. Downloaded on 6/3/2026 9:25:06 AM. This article is licensed under a Creative Commons Attribution-NonCommercial 3.0 Unported Licence.

carboxylate groups. In this case, the pyridine donors would be displaced slightly above and below the equatorial plane to minimize steric repulsion between them. The somewhat smaller $g_{\|}$ values observed in our spectra are also consistent with this model, reflecting the stronger ligand field exerted by nitrogen donors compared to oxygen. Such geometry has also been confirmed by single-crystal X-ray diffraction for [Cu(CRpy$_2$)],[51] whose EPR parameters reported in frozen DMF solvent (150 K) were found to be close to those measured for $[Cu(DO2S2Py)]^{2+}$. Deviations from an ideal elongated octahedral geometry (*e.g.*, donor atoms bound to copper ions deviate from the equatorial plane or the axial donor groups forming angles smaller than 90° with the equatorial plane) contribute to strong rhombicity and the resulting spectral broadening.

The EPR spectrum of $[Cu(DO2S2Py)]^{2+}$ at room temperature (Fig. S27) can be simulated by averaging the anisotropic parameters obtained from the frozen-state analysis. As in the frozen spectrum, the room temperature signal is also extremely broad, which is partly due to the relatively small copper hyperfine coupling constant. In addition, the rotational correlation time of 4.2×10^{-10} s suggests slow molecular tumbling, likely caused by steric hindrance from the non-coordinating side arms, which impede rotational motion.

To obtain further insights into the structures of the complexes formed by coordination of the DO2S2Py ligand, quantum mechanical DFT calculations were performed. All the relevant coordination geometries of DO2S2Py with Cu^{2+}, as well as Cu^{+} and Ag^{+}, were explored to identify the preferred coordination modes for each metal ion and to rationalize the experimentally observed behavior. The fully deprotonated form of DO2S2Py was considered in all the calculations.

Based on our simulations, the most stable structures were obtained when the metal was inserted into the cavity of the DO2S2Py ligand. All the optimized structures of the Cu^{2+} metal complexes are shown in Fig. S28 along with their Gibbs free energies (ΔG) calculated in water (Table 3). The most important distances between the ligand and the metals are reported in Table S4.

Upon coordination of Cu^{2+}, all the computed structures exhibit high stability, indicating that the ligand has a strong affinity for the metal center, in agreement with experimental observations. The most stable structure is obtained when the Cu^{2+} cation is placed in the middle of the macrocycle but slightly displaced above the cavity, forming strong coordination bonds with three nitrogen atoms of the macrocyclic core (N_{cy}) and with the two pyridine nitrogen atoms (N_{py}). A weaker interaction is established with the fourth nitrogen atom of the macrocycle. This coordination mode is denoted as [Cu^{2+}–$4N_{cy}2N_{py}$]. The resulting coordination geometry confirms experimental findings of a distorted elongated octahedral arrangement, with the two pyridine nitrogens lying within the equatorial plane, whereas two nitrogen atoms of the macrocycle occupy the axial position.

The calculated electronic spectrum for this configuration closely reproduces the experimental one reported in Fig. S18. The optimized structure of the [Cu^{2+}–$4N_{cy}2N_{py}$] complex, together with its UV-Vis spectrum, computed using the same theoretical protocol, is reported in Fig. 6. The electronic transitions describing the absorption spectrum were fully characterized and are collected in Table S5. The Gibbs free energy calculated for the formation of [Cu^{2+}–$4N_{cy}2N_{py}$] species is −34.3 kcal mol^{-1} (Table 3), corresponding to a logβ value of 25.1. This calculated value is in surprisingly good agreement with the experimental logβ of 23.6 ± 0.07 (Table 1).

For the geometry denoted as [Cu^{2+}–$4N_{cy}1N_{py}$], in which the metal, lying in the center of the cyclen backbone, is simultaneously coordinated to the four ring nitrogen atoms and one pyridine ligand, the calculated free energy is −32.9 kcal mol^{-1} (Table 3), corresponding to a logβ value of 24. DFT calculations, therefore, do not completely rule out the coexistence of multiple stable coordination modes of the ligand in aqueous solution.

A third stable complex was computationally identified, indicated as [Cu^{2+}–$4N_{cy}1S$], that exhibits a Gibbs free energy of formation of −25.2 kcal mol^{-1} (Table 3) and a corresponding logβ value of 18.5. Unlike the species described previously, this complex involves the coordination of one of the sulfur atoms from the pendant arms, which results in an evident minor stability. The soft character of the sulfur atom, and its lower σ-donation ability compared to nitrogen-based donors, likely contribute to the lower affinity of this ligand toward the Cu^{2+} metal ion. In the fourth and least stable configuration, [Cu^{2+}–$4N_{cy}$], all pendant arms of DO2S2Py are oriented away from the metal center, leaving Cu^{2+} coordinated exclusively to the four nitrogen atoms of the macrocyclic cavity. This geometry can be classified as a pseudo square-planar arrangement with no axial donor interactions. The calculated Gibbs free energy for this species is −31.9 kcal mol^{-1} (Table 3), corresponding to a logβ value of 23.4. For all the optimized structures, the calculated Gibbs free energies indicate a good stability of the formed complexes, and all the corresponding electronic spectra were calculated. Among them, only the spectrum of the complex named [Cu^{2+}–$4N_{cy}2N_{py}$], reported in Fig. 6, closely matches the experimental one.

Table 3 Gibbs free energies (ΔG) calculated in water for the different coordination modes of the Cu^{2+}, Cu^{+}, and Ag^{+} complexes of DO2S2Py

Metal ion	Coordination mode	ΔG [kcal mol^{-1}]
Cu^{2+}	$4N_{cy}2N_{py}$	−34.3
	$4N_{cy}1N_{py}$	−32.9
	$4N_{cy}$	−31.9
	$4N_{cy}1S$	−25.2
Cu^{+}	$3N_{cy}1N_{py}$	−26.1
	$3N_{cy}1S$	−24.2
	$4N_{cy}$	−23.2
Ag^{+}	$4N_{cy}1N_{py}1S$	−21.7
	$4N_{cy}2N_{py}$	−21.3
	$4N_{cy}2S$	−17.5

2.5.2. Ag^{+}-DO2S2Py. Differently from the Cu^{2+} system, in presence of Ag^{+}, NMR is a powerful technique to elucidate chemical structure in solution. In the ^{1}H NMR spectrum of

This journal is © the Partner Organisations 2026

Open Access Article. Published on 23 April 2026. Downloaded on 6/3/2026 9:25:06 AM.
This article is licensed under a Creative Commons Attribution-NonCommercial 3.0 Unported Licence.

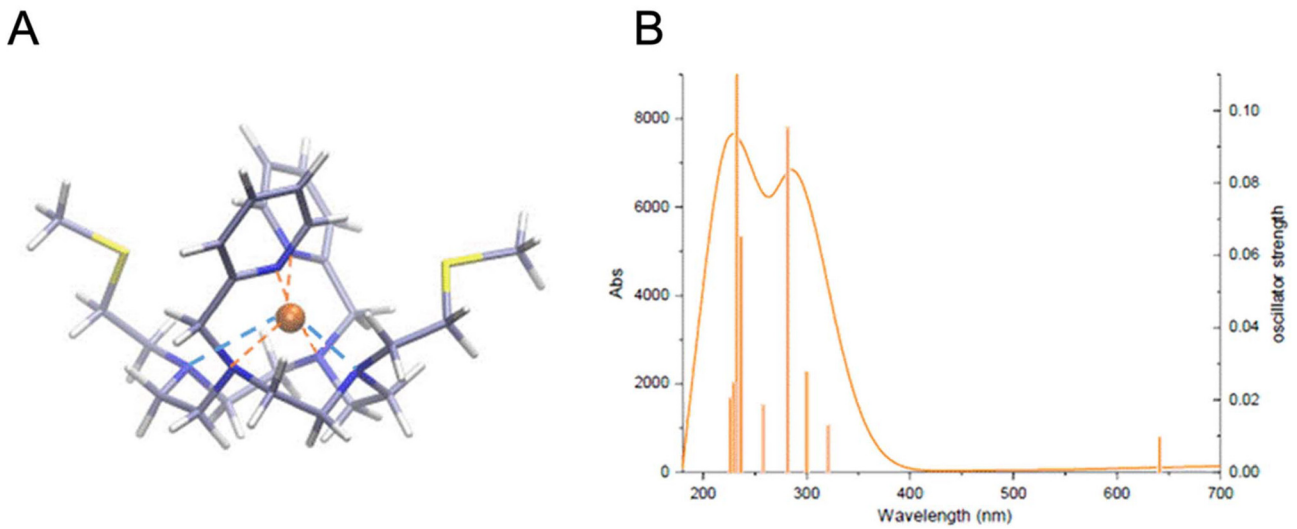

Fig. 6 (A) DFT optimized geometry of the most stable structure of $[Cu(DO2S2Py)]^{2+}$, namely $[Cu^{2+}–4N_{cy}2N_{py}]$ and (B) the corresponding calculated TDDFT absorption spectrum.

$[Ag(DO2S2Py)]^+$, the aliphatic protons (H_1, H_2, H_3, and H_4) appear as extremely broad singlets, while the aromatic protons show the expected multiplicities: doublets for H_6 and H_9 and triplets for H_7 and H_8 (Fig. 7). Each set of chemically equivalent protons giving rise to a single resonance indicates that the opposite side arms, which are identical in structure, are also magnetically equivalent in solution upon metal coordination.

Comparison of the ^1H NMR spectrum of $[Ag(DO2S2Py)]^+$ with that of the free ligand bearing the same net charge (HL^+) provides important insights into the solution structures of this complex (Fig. 7). The pyridine protons (H_6–H_9) are consistently deshielded in $[Ag(DO2S2Py)]^+$ compared to the free ligand. A similar downfield shift is observed for the SCH_3 and SCH_2 protons (H_1 and H_2) and the NCH_2 protons connecting the cyclen backbone to the pyridine arms (H_5). In contrast, the aliphatic N-bound protons on the macrocyclic backbone (H_3 and H_4) experience an overall upfield shift. These variations are consistent with coordination-induced electronic effects: deshielding near the metal due to its electron-withdrawing nature and shielding on the nitrogen-bound protons due to increased electron density upon metal coordination. Indeed, in the free ligand, protonation is localized on the amines, which leads to relatively lower electron density in these protons. In contrast, in the complexes, Ag^+ likely interacts simultaneously with both nitrogen and sulfur donors, redistributing electron density and shielding the N-bound protons. Similar trends have been previously reported for Ag^+ complexes of analogous sulfur-containing ligands.[42,43]

Collectively, the combination of chemical shift changes and the presence of single resonances for each set of chemically equivalent protons of $[Ag(DO2S2Py)]^+$ indicates that all donors are, on average, involved in the metal binding. The data further suggests

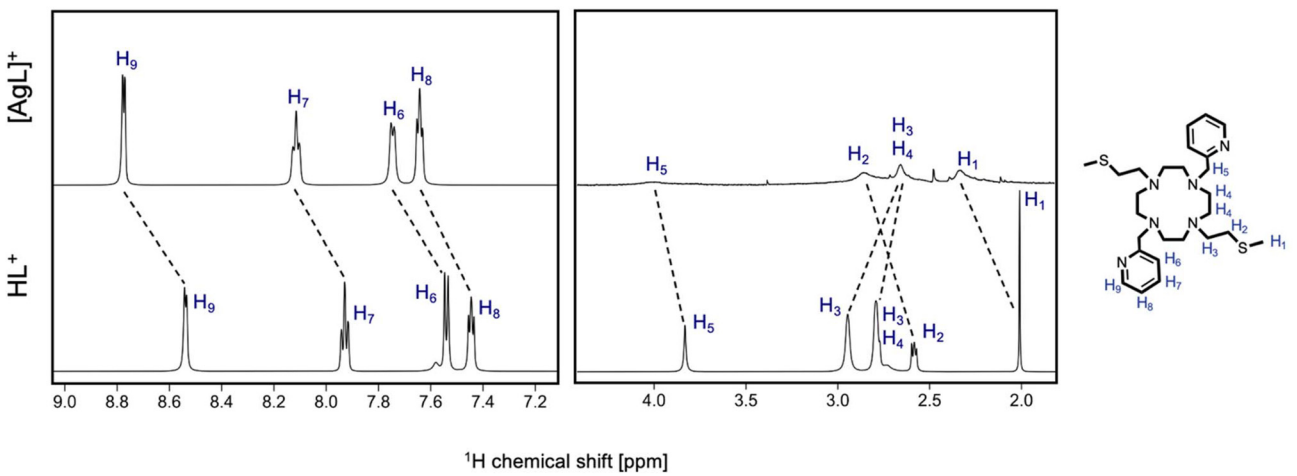

Fig. 7 Comparison of ^1H NMR spectra of $[Ag(DO2S2Py)]^+$ and free DO2S2Py (HL^+ form) (400 MHz, D_2O, T = 25 °C).

Open Access Article. Published on 23 April 2026. Downloaded on 6/3/2026 9:25:06 AM.
This article is licensed under a Creative Commons Attribution-NonCommercial 3.0 Unported Licence.

a dynamic binding regime, in which the donor atoms undergo rapid binding–unbinding events. In particular, the sulfur-containing side arms appear to experience relatively slow-exchange dynamics, as evidenced by their very broad resonances (almost approaching coalescence), whereas the pyridine donors are in fast exchange, resulting in averaged and relatively sharp signals. This fluxional behavior highlights that a flexible coordination mode is favored when Ag^+ is confined in a highly dentate macrocyclic scaffold, as previously observed with similar systems.[42,43]

To support NMR data and clarify coordination geometry of Ag^+, DFT computations were performed. Fig. S29 reports all the optimized molecular structures for $[Ag(DO2S2Py)]^+$, along with their corresponding Gibbs free energies (ΔG) calculated in aqueous solution. In line with experimental observations, Ag^+ forms less stable coordination complexes compared to Cu^{2+}, with the metal located inside the macrocyclic cavity but weakly bound, as indicated by the coordination bond lengths exceeding 2.5 Å. This behavior is reflected in the Gibbs free energy value for the complex formation, which increases by approximately +10 kcal mol^{-1} in presence of Ag^+ rather than Cu^{2+} (Table 3). The two most stable configurations were identified, which have similar formation free energies, but different structural features (Fig. 8).

The first one, denoted as $[Ag^+–4N_{cy}1N_{py}1S]$, has a Gibbs free energy of −21.7 kcal mol^{-1} (Table 3) corresponding to a logβ of 15.9. In this species, the Ag^+ ion is located inside the cyclen backbone and coordinates the four nitrogen atoms of the macrocycle, one pyridine nitrogen and one sulfur-containing side arm. The second configuration, named $[Ag^+–4N_{cy}2N_{py}]$, is slightly less stable and features the coordination of all nitrogen atoms of DO2S2Py to the metal. The calculated Gibbs free energy is −21.3 kcal mol^{-1} (Table 3) corresponding to a logβ of 15.6. Both complexes are therefore predicted to be formed in aqueous solution, with logβ values close to the experimentally reported one of 16.94.

When both sulfur atoms, even if softer than nitrogen, are coordinated to Ag^+, a decrease in free energy and logβ is observed (Fig. S29). For this configuration, named $[Ag^+–4N_{cy}2S]$, the Gibbs free energy is −17.5 kcal mol^{-1} (Table 3) and the calculated logβ is 12.8.

2.6. Dissociation kinetics of DO2S2Py complexes

The thermodynamic stability of a radiometal complex is a critical requirement for its use in radiopharmaceutical applications. However, once administered *in vivo*, the complex is exposed to a dynamic and competitive biological environment where various endogenous species may challenge the integrity of the complex. These non-equilibrium conditions may lead to demetallation events from the chelator, resulting in the release of the metal ion and its potential accumulation in non-target

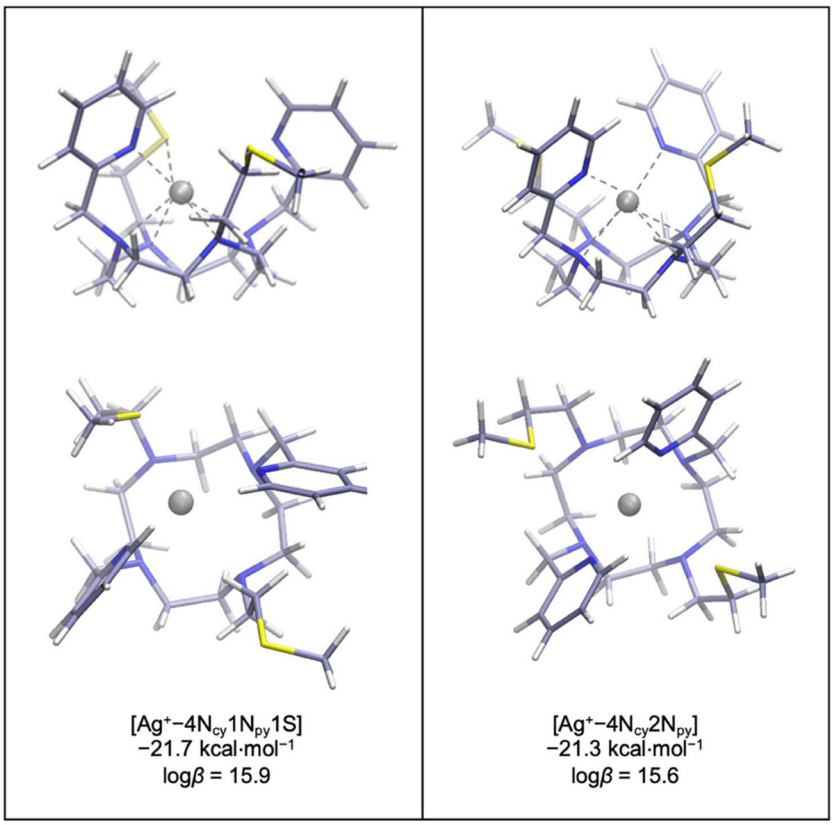

Fig. 8 DFT optimized geometries of the most stable structures of $[Ag(DO2S2Py)]^+$ calculated in water together with the relative binding energies (kcal mol^{-1}).

This journal is © the Partner Organisations 2026

Open Access Article. Published on 23 April 2026. Downloaded on 6/3/2026 9:25:06 AM. This article is licensed under a Creative Commons Attribution-NonCommercial 3.0 Unported Licence.

tissues. Consequently, different experiments were conducted to assess the kinetic inertness of the investigated Cu^{2+} and Ag^{+} complexes.

2.6.1. Kinetic inertness in presence of biologically relevant ions. Challenge experiments were conducted using physiologically relevant cations (Mg^{2+}, Ca^{2+} and Zn^{2+}) as well as phosphate buffer (pH 7.4) to mimic the conditions of biological fluids.

Representative time-dependent UV-Vis spectra for $[Cu(DO2S2Py)]^{2+}$ in different competitive media are shown in Fig. S30. Notably, no significant spectral changes were observed over 24 hours, indicating that $[Cu(DO2S2Py)]^{2+}$ is inert under these conditions and that DO2S2Py does not form stable complexes with the selected competing cations, as no spectral changes relative to the free ligand were observed upon addition of these ions. Furthermore, the complex remained stable in phosphate-buffered saline (PBS), further supporting its high kinetic robustness under physiological conditions. A similar behavior was observed for the Ag^{+} counterpart, as illustrated in Fig. S31. No evidence of demetallation or complex degradation was detected over time, underscoring the exceptional inertness of this complex.

2.6.2. Kinetic inertness under acidic conditions. The acid-induced decomplexation kinetics of $[Cu(DO2S2Py)]^{2+}$ and $[Ag(DO2S2Py)]^{+}$ were assessed by incubating the pre-formed complexes in strongly acidic media (pH $\ll$ 2). Although such extreme conditions are not physiologically relevant, this assay provides a stringent test of kinetic inertness and allows quantitative comparisons with other chelators under harsh conditions.

Representative changes in the electronic spectra of $[Cu(DO2S2Py)]^{2+}$ upon incubation in increasingly acidic solutions are shown in Fig. S32 and the corresponding dissociation half-lives ($^{d}t_{1/2}$) are reported in Table S6. The observed first-order dissociation rate constants ($^{d}k_{obs}$) exhibit a linear dependence on proton concentration (Fig. S33), suggesting that only one complex undergoes dissociation and that the protonation constant of the predissociation step is low.[40] Accordingly, the second-order rate constant (^{d}k) was derived using the relationship $^{d}k_{obs} = {}^{d}k[H^{+}]$.

A comparison with ^{d}k values for other sulfur-containing chelators is provided in Table 4. Based on the data, the kinetic inertness of the Cu^{2+} complexes follows the order: DO2A2S > DO2S2Py ≈ DO4S ≫ TE4S. This indicates that the inclusion of both sulfur- and pyridine-containing pendant arms on a cyclen backbone does not enhance the kinetic inertness of the complex against acid-induced dissociation, which on the other hand is enhanced in the presence of negatively charged groups such as the acetate of DO2A2S. However, this ranking reflects behavior under highly acidic conditions and may not directly translate to *in vivo* environments, where such extreme acidity is not encountered. Therefore, other tests such as the human serum stability were conducted (see below).

The decomplexation kinetics of the Ag^{+} counterpart were only qualitatively evaluated. Indeed, upon dissolution of $[Ag(DO2S2Py)]^{+}$ in highly acidic conditions (pH $\ll$ 2), the ^{1}H NMR spectrum changes immediately, becoming identical to that of the free ligand with no further spectral changes over time. This observation suggests that the Ag^{+} complex is significantly more labile under these conditions than its Cu^{2+} counterpart. This difference likely arises from the intrinsic electronic characteristics of the two metals: Ag^{+} is a d^{10} ion, generally more labile, while Cu^{2+} is a d^{9} ion, forming more inert complexes.

2.6.3. Copper reduction. A potential decomplexation pathway for Cu^{2+} complexes *in vivo* involves the reduction of Cu^{2+} to Cu^{+} by endogenous bioreductants, followed by dissociation from the chelator and subsequent transchelation to endogenous Cu^{+}-binding proteins. To investigate the ability of DO2S2Py to bind Cu^{+}, DFT calculations were carried out. All the optimized geometries for the complexes formed by the Cu^{+} ion and DO2S2Py are reported in Fig. S34, and the most relevant bond distances are summarized in Table S4.

The theoretical results indicate that DO2S2Py can coordinate the Cu^{+} center, but the resulting complexes are approximately 10 kcal mol^{-1} less stable than the corresponding Cu^{2+} complexes (Table 3). Several attempts were made to explore in detail all the possible coordination modes, but only three distinct configurations were identified. In all cases, Cu^{+} is located within the macrocyclic cavity. In the first geometry, designated as $[Cu^{+}–3N_{cy}1N_{py}]$, the copper center forms three coordination bonds with three nitrogen atoms of the macrocyclic ring and additionally coordinates one of the two pyridine donors. In the second geometry, identified as $[Cu^{+}–3N_{cy}1S]$, the coordination of the pyridine nitrogen is replaced by the sulfur atom from one pendant arm.

The calculated free energy for the former is −26.1 kcal mol^{-1}, corresponding to logβ = 19.1, whereas for the latter the free energy is −24.2 kcal mol^{-1} with logβ = 17.7 (Table 3). In the third configuration, denoted as $[Cu^{+}–4N_{cy}]$, the Cu^{+} center coordinates all four donor atoms of the cyclen ring, but this arrangement is approximately 3 kcal mol^{-1} less stable than the most favorable geometry (Table 3). The corresponding free energy is −23.2 kcal mol^{-1} (Table 3), corresponding to logβ = 17.0. The reduced stability of the Cu^{+} complexes compared to the Cu^{2+} analogues can be rationalized in terms of a reduced macrocyclic effect, a trend widely reported in the literature for this metal center.[54] Under these conditions, Cu^{+} preferentially adopts a coordination number of four, and realizing this geo-

Table 4 Comparison of the acid-assisted dissociation kinetic constant (^{d}k) of $[Cu(DO2S2Py)]^{2+}$ and Cu^{2+} complexes of other sulfur-containing chelators[40]

	DO4S	DO2A2S	TE4S	DO2S2Py
^{d}k [M^{-1} s^{-1}]	$(5.7 \pm 0.1) \times 10^{-4}$	$(1.04 \pm 0.02) \times 10^{-4}$	$\sim 10^{-2}$	$(5.32 \pm 0.05) \times 10^{-4}$

Open Access Article. Published on 23 April 2026. Downloaded on 6/3/2026 9:25:06 AM. This article is licensed under a Creative Commons Attribution-NonCommercial 3.0 Unported Licence.

metry requires several structural adjustments within the chelator to maximize the metal–ligand interactions.

Cyclic voltammetry (CV) was performed, and the resulting voltammograms are shown in Fig. S35. Unexpectedly, the voltammogram of $[Cu(DO2S2Py)]^{2+}$ displayed an irreversible reduction signal located at approximately −0.5 V. In the reverse scan, the voltammogram instead shows a peak at around 0.05 V, very close to the oxidation peak of free Cu^{+} in solution.[38] This suggests that the ligand is unable to effectively stabilize the reduced Cu^{+} species.

This voltammetric behavior appears surprising given that DO2S2Py can bind Ag^{+} and that DFT calculations support the formation of stable complexes with Cu^{+} as well. We hypothesize that, upon reduction, the ligand cannot reorganize rapidly enough to enable an effective coordination by the softer sulfur donors, likely due to steric hindrance and the conformational rigidity imposed by the bulky pyridine groups. This behavior contrasts with that of other sulfur-containing chelators, such as DO2A2S and DO4S, which have been shown to stabilize both oxidation states of copper.[38] However, a similar lability is often observed in the literature with other cyclen-based chelators.[50,51]

2.7. Radiolabeling of DO2S2Py

2.7.1. $[^{64}Cu]Cu^{2+}$. Concentration- (10^{-4} M < C < 10^{-8} M), time- (5 min < t < 60 min), pH- (4.5 and 7), and temperature-dependent (RT and 95 °C) radiolabeling experiments with $[^{64}Cu]Cu^{2+}$ were conducted. The results are summarized in Fig. 9.

At pH 4.5, quantitative radiochemical yields (RCY > 99%) were obtained at a maximum apparent molar activity (AMA_{max}) of 1 MBq nmol^{-1} (corresponding to a $C_{DO2S2Py}$ = 10^{-5} M) both at room temperature and 95 °C. Notably, no significant differences in the achievable AMA_{max} were observed upon extending the reaction time from 5 min to 60 min. Indeed, when the chelator concentration was reduced to 10^{-6} M and 10^{-7} M, the RCY dropped below 50% and 10%, respectively, highlighting a limit in the achievable apparent molar activity under these conditions.

At pH 7, quantitative RCY > 95% was achieved at room temperature within 5 min at AMA_{max} = 1 MBq nmol^{-1} ($C_{DO2S2Py}$ = 10^{-5} M). Also in this case, prolonged incubation did not increase the AMA_{max} that remained limited to 1 MBq nmol^{-1}. In contrast, heating the reaction mixture at 95 °C

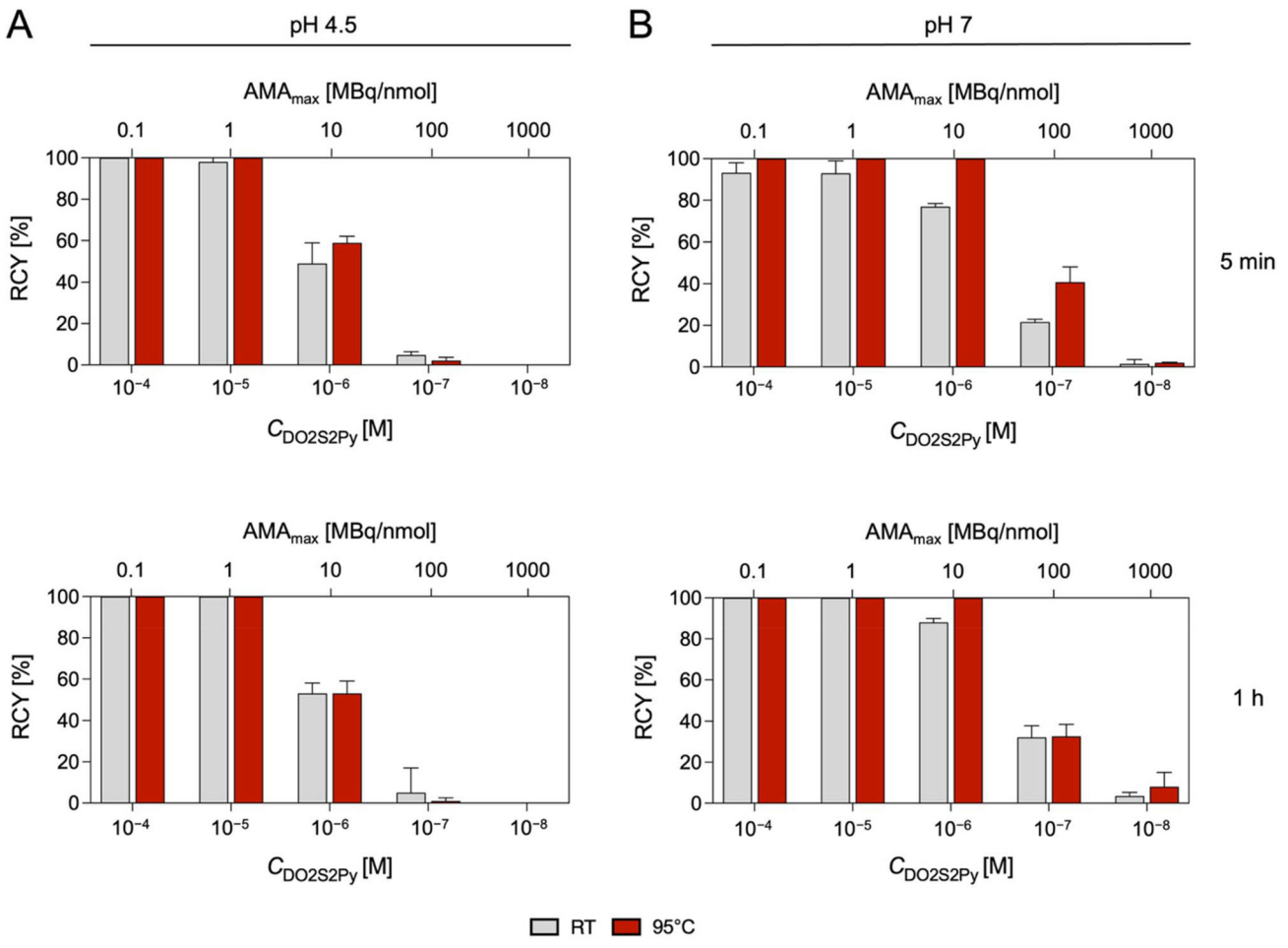

Fig. 9 Concentration-, time-, and temperature-dependent $[^{64}Cu]Cu^{2+}$ radiolabeling with DO2S2Py at (A) pH 4.5 and (B) pH 7.

This journal is © the Partner Organisations 2026

Open Access Article. Published on 23 April 2026. Downloaded on 6/3/2026 9:25:06 AM. This article is licensed under a Creative Commons Attribution-NonCommercial 3.0 Unported Licence.

enabled a tenfold increase in apparent molar activity (AMA_{max} = 10 MBq nmol^{-1}, $C_{DO2S2Py}$ = 10^{-6} M) with respect to ambient temperature. No impact on the reaction time was observed.

The differences observed between the two investigated pH values are consistent with previous results obtained using analogous sulfur-rich chelators.[39,41] These changes are attributed to the lower degree of protonation of the chelator at higher pH, which facilitates complexation by reducing electrostatic repulsion between the protonated donor sites and the incoming [^{64}Cu]Cu^{2+} ions.

Compared to one of the current standards for radiocopper chelation, NOTA, DO2S2Py shows a similar performance at both pH values (Fig. S36). In contrast, when evaluated against previously reported sulfur-rich cyclen-based chelators (*e.g.*, DO4S and DO2A2S), DO2S2Py performs at a comparable or slightly lower level. However, this apparent discrepancy may arise from the use of different copper batches in the respective experiments.[39]

2.7.2. [^{111}Ag]Ag^{+}. Radiolabeling experiments were performed with [^{111}Ag]Ag^{+}, investigating the influence of chelator concentration (10^{-4} M < C < 10^{-7} M), reaction time (5 min and 60 min), and temperature (RT and 95 °C). Due to the limited availability of [^{111}Ag]Ag^{+}, only one pH condition (pH 7.4) was tested, selected on the basis of the reaction conditions optimized in our previous works.[42,43] The results are reported in Fig. 10.

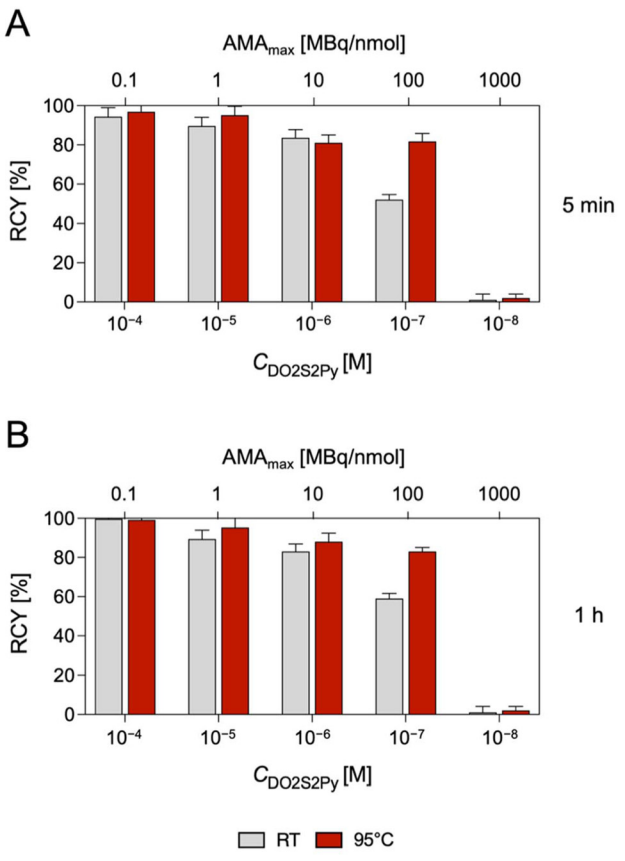

Fig. 10 Concentration- and temperature-dependent [^{111}Ag]Ag^{+} radiolabeling with DO2S2Py at pH 7.4 after (A) 5 min and (B) 60 min.

Quantitative radiometal incorporation was achieved up to 0.1 MBq nmol^{-1} within 5 min. The RCY dropped to approximately 50% at 100 MBq nmol^{-1}. Heating the reaction mixture to 95 °C significantly enhanced the radiolabeling efficiency, increasing the AMA_{max} to 1 MBq nmol^{-1}. Extending the reaction time did not produce appreciable improvement in the radiometal incorporation.

Under these conditions, the AMA_{max} attained was 1 MBq nmol^{-1}, roughly one order of magnitude lower than that observed with [^{64}Cu]Cu^{2+}. However, this difference may reflect varying levels of metal impurities between the two radioisotopes, which can influence complexation behavior. Consequently, no definitive conclusions regarding chelator selectivity or preference can be drawn. Nonetheless, the results indicate that the chelator exhibits strong affinity for both radiometals. Compared to DO4S, the performance of DO2S2Py appears slightly inferior (Fig. S37).

2.8. *In vitro* stability in biological media of [^{64}Cu][Cu(DO2S2Py)]$^{2+}$ and [^{111}Ag][Ag(DO2S2Py)]$^{+}$

As the final step in evaluating DO2S2Py as a chelator for copper and silver radioisotopes, the *in vitro* stability of the corresponding radioactive complexes was assessed in PBS and human serum.

As illustrated in Fig. 11, [^{64}Cu][Cu(DO2S2Py)]$^{2+}$ showed excellent stability under both conditions, with no detectable radiometal release and retention of >95% integrity after 24 h. [^{111}Ag][Ag(DO2S2Py)]$^{+}$ displayed lower stability compared to its copper analogue: after 24 h, it maintained ~90% integrity in PBS, while it dropped to ~75% in human serum. The modest decomplexation observed in PBS likely reflects competitions with chloride ions, while the further stability decline in serum is probably caused by interactions with serum components (*e.g.*, albumin). However, it is important to note that [^{111}Ag][Ag(DO2S2Py)]$^{+}$ outperformed the previously best-performing chelator for silver radioisotopes (DO4S), underscoring the beneficial effect of incorporating pyridine arms (Fig. S38). These additional donor groups appear to provide enhanced shielding of the metal center, thereby reducing susceptibility to competing biological ligands.

3. Experimental

3.1. General

All solvents and reagents were purchased from commercial suppliers (Sigma-Aldrich, Aristar – VWR Chemicals, EMSURE, Merck, Chematech, Macrocyclics) and used without further purification. Ultrapure water (18.2 MΩ cm^{1}) was obtained from a Milli-Q purification system and used throughout.

Organic reactions were monitored by thin-layer chromatography (TLC) on aluminum plates coated with silica gel 60 F_{254} (Merck). Flash column chromatography was performed using high-purity silica gel (60 Å, 230–400 mesh, 40–63 μm, Merck), with the appropriate eluents, as described in the corres-

Open Access Article. Published on 23 April 2026. Downloaded on 6/3/2026 9:25:06 AM.
This article is licensed under a Creative Commons Attribution-NonCommercial 3.0 Unported Licence.

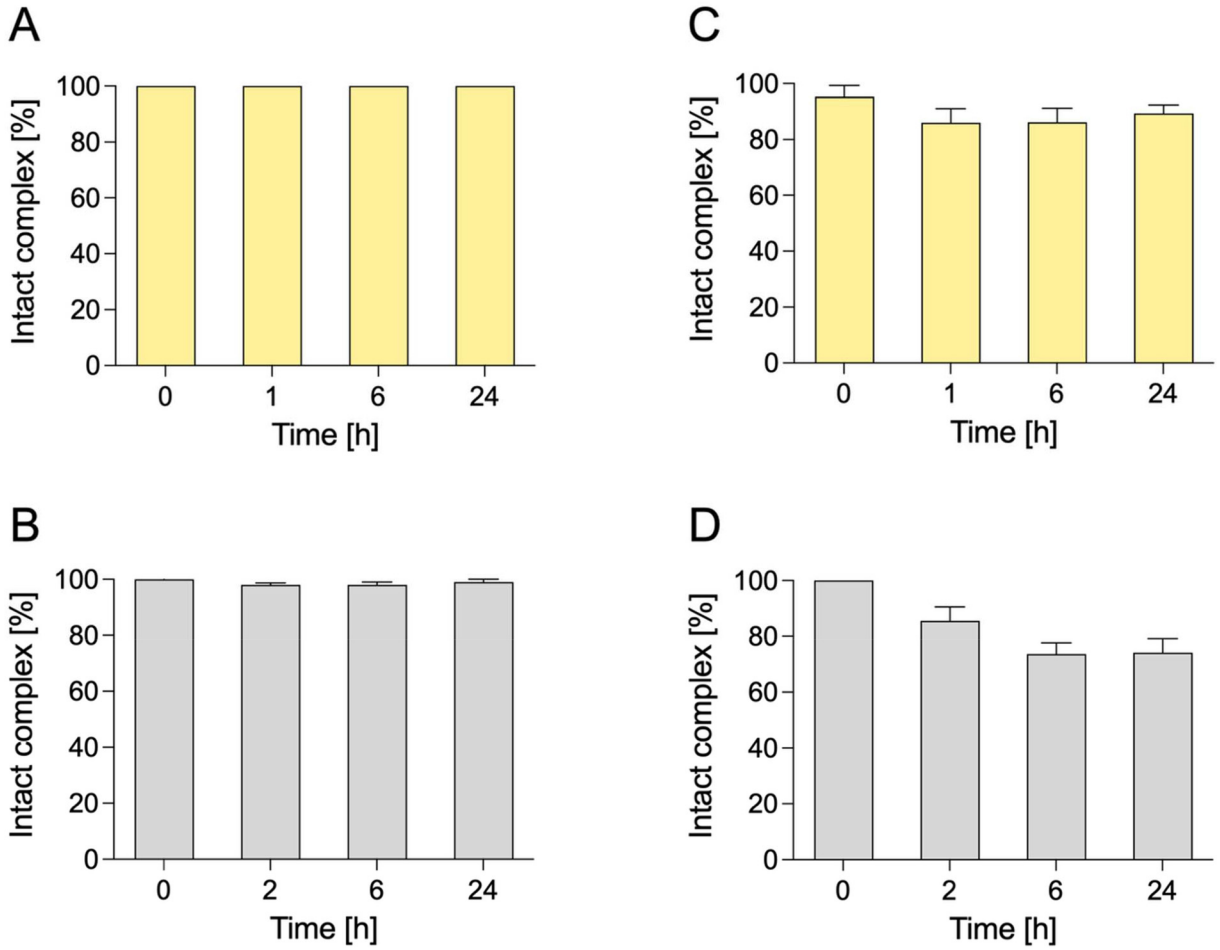

Fig. 11 Integrity of (A, B) $[^{64}Cu][Cu(DO2S2Py)]^{2+}$ and (C, D) $[^{111}Ag][Ag(DO2S2Py)]^{+}$ in PBS (A and C) and human serum (B and D) (1 : 1 V/V dilution).

ponding section. The final product (DO2S2Py) was purified by reverse-phase semipreparative high-performance liquid chromatography (RP-HPLC) using a Phenomenex Luna C18 (150 mm × 100 mm) column. NMR spectra were recorded on a Bruker AVANCE AMX 400 spectrometer (^{1}H: 400.12 MHz; ^{13}C: 100.13 MHz) or a Bruker AVANCE AMX 600 spectrometer equipped with a CryoProbe BBO H&F 5 mm in inverse detection (^{1}H: 600.13 MHz, ^{13}C: 150.13 MHz). ^{1}H and $^{13}C\{^{1}H\}$ NMR spectra are reported on the chemical shifts (δ) scale and referenced to residual solvent peaks or 3-(trimethylsilyl)propionic acid sodium salt (TSP) in D_2O. Signal multiplicity is reported as follows: s = singlet, d = doublet, t = triplet, br = broad peak, m = multiplet. Mass spectrometry (MS) analyses were performed on an Agilent 6210 TOF LC/MS, an Advion expression LC-MS, or an Agilent 6300 Ion Trap LC-MS system equipped with an electrospray (ESI) source. The pH was measured with a Mettler Toledo SevenEasy pH-meter and a Crison (pH 0–14) combined glass electrode. UV-Vis spectra were recorded on a JASCO V-770 UV/Vis/NIR spectrophotometer over the 200–800 nm spectral range, using quartz cells with 1 cm optical path. EPR spectra were acquired with a Bruker EleXsys E500 spectrometer. CV measurements were carried out using an Autolab PGSTAT-30 potentiostat, under the control of GPES software. Unless otherwise stated, no uncommon hazards were noted during the experiments.

3.2. Synthesis

3.2.1. 1,7-Bis(*tert*-butyloxycarbonyl)-1,4,7,10-tetraazacyclododecane (di-Boc-cyclen). Under Ar atmosphere, cyclen (400 mg, 2.32 mmol, 1.0 eq.) was dissolved in dry methanol (20 mL). The solution was cooled in an ice bath, and *N*-Boc-succinimide (Boc-OSu, 1.00 g, 4.65 mmol, 2.0 eq.), previously dissolved in methanol (2 mL), was added dropwise over 30 min. The reaction mixture was then allowed to warm to room temperature and stirred overnight. After completion, the solvent was removed under reduced pressure. The resulting residue was redissolved in 3 M NaOH and extracted with chloroform (3×). The combined organic layers were dried over anhydrous Na_2SO_4, filtered through a cotton plug, and concentrated under reduced pressure. The crude product was purified by flash column chromatography on silica gel using a mixture of isopropanol and aqueous ammonia (8 : 2) as eluent to afford di-Boc-cyclen as a colorless oil (520.8 mg, yield = 60%). ^{1}H NMR (400 MHz, $CDCl_3$, 25 °C) δ (ppm): 3.26 (t, 8 H, NCH_2),

This journal is © the Partner Organisations 2026

Open Access Article. Published on 23 April 2026. Downloaded on 6/3/2026 9:25:06 AM. This article is licensed under a Creative Commons Attribution-NonCommercial 3.0 Unported Licence.

3.03 (s, 2 H, NH), 2.76 (t, 8 H, NCH_2), 1.37 (s, 18 H, CH_3). ESI-MS: *m*/*z* 373.28 (found); 373.28 (calc. for $[C_{18}H_{37}N_4O_4]^+$).

3.2.2. 1,7-Bis(*tert*-butyloxycarbonyl)-4,10-bis(2-(methylsulfanyl)ethyl)-1,4,7,10 tetraazacyclododecane (di-Boc-DO2S). Di-Boc-cyclen (447.0 mg, 1.2 mmol, 1 eq.) was dissolved in dry acetonitrile (40 mL) under Ar atmosphere. K_2CO_3 (1.79 g, 12.96 mmol, 8 eq.) was added, followed by the addition of 2-chloroethylmethyl sulfide (641 µL, 6.44 mmol, 4 eq.). The reaction mixture was heated at 50 °C for 2 days. After cooling to room temperature, the mixture was filtered through filter paper, and the solvent was removed under reduced pressure. The crude mixture was purified by flash column chromatography on silica gel using a gradient of dichloromethane/methanol (from 99 : 1 + 1% NH_3 to 95 : 5 + 1% NH_3). The desired product, di-Boc-DO2S, was obtained as a light-yellow oil (210.5 mg, 33% yield). ^{1}H NMR (400 MHz, $CDCl_3$, 25 °C) δ (ppm): 3.34 (s, 8 H, NCH_2), 2.67 (t, 12 H, NCH_2), 2.54 (t, 4 H, SCH_2), 2.09 (s, 6 H, SCH_3), 1.43 (s, 18 H, CH_3). ^{13}C NMR (400 MHz, $CDCl_3$, 25 °C) δ (ppm): 156.0 (C=O), 79.5 (–$\underline{C}(CH_3)$), 54.3 + 54.7 (NCH_2), 46.8 (NCH_2), 31.5 (SCH_2), 28.6 (CH_3), 15.9 (SCH_3). ESI-MS: *m*/*z* 521.32 (found); 521.32 (calc. for $[C_{24}H_{49}N_4O_4S_2]^+$).

3.2.3. 1,7-Bis(2-(methylsulfanyl)ethyl)-1,4,7,10-tetraazacyclododecane (DO2S). Di-Boc-DO2S (150 mg) was dissolved in dichloromethane (9 mL), and trifluoroacetic acid (TFA, 10% in dichloromethane) was added dropwise (3 mL) at room temperature. The reaction mixture was stirred overnight. After completion, the solvent was removed under reduced pressure, and the residue was co-evaporated with toluene (3×) to remove residual TFA. DO2S was obtained as a yellow oil (160 mg, quantitative yield). ^{1}H NMR (400 MHz, $CDCl_3$, 25 °C) δ (ppm): 2.60–2.55 (m, 24 H, NCH_2 + SCH_2), 2.05 (s, 6 H, SCH_3). ^{13}C NMR (400 MHz, $CDCl_3$, 25 °C) δ (ppm): 53.8 (NCH_2), 52.1 (NCH_2), 45.3 (NCH_2), 32.8 (SCH_2), 15.7 (SCH_3). ESI-MS: *m*/*z* 321.21 (found); 321.21 (calc. for $[C_{14}H_{33}N_4S_2]^+$).

3.2.4. 1,7-Bis(2-(methylsulfanyl)ethyl)-4,10-bis(pyridin-2-ylmethyl)-1,4,7,10-tetraazacyclododecane (DO2S2Py). DO2S·2TFA (98.1 mg, 0.18 mmol, 1 eq.) was dissolved in dry acetonitrile (10 mL) under Ar atmosphere. K_2CO_3 (138 mg, 1 mmol, 5 eq.) was added, followed by the dropwise addition of 2-(bromomethyl)pyridine hydrobromide (136 mg, 0.54 mmol, 3 eq.) dissolved in acetonitrile (1 mL). The reaction mixture was stirred at room temperature for 3 days. The solvent was removed under reduced pressure, and the crude product was purified by HPLC to afford DO2S2Py as a yellow oil (34.8 mg, yield 38%). ^{1}H NMR (400 MHz, D_2O, 25 °C) δ (ppm): 8.51 (d, 2 H, H_{Py}), 7.89 (t, 2 H, H_{Py}), 7.49 (d, 2 H, H_{Py}), 7.41 (t, 2 H, H_{Py}), 3.81 (s br, 4 H, NCH_2), 2.93 (s br, 8 H, NCH_2) + 2.76 (s br, 12 H, NCH_2), 2.55 (t, 4 H, SCH_2), 1.97 (s, 6 H, SCH_3). ^{13}C NMR (400 MHz, D_2O, 25 °C) δ (ppm): 171.1 (C_{py}), 148.6 (C_{py}), 138.3 (C_{py}), 125.1 (C_{py}), 123.7 (C_{py}), 60.0 (NCH_2), 51.3 + 48.3 (NCH_2), 26.4 (SCH_2), 14.5 (SCH_3). ESI-MS: *m*/*z* 503.26 (found); 503.30 (calc. for $[C_{26}H_{43}N_6S_2]^+$).

3.3. Coordination chemistry

3.3.1. General. Stock solutions of DO2S2Py were prepared by dissolving a weighed amount of ligand directly in Milli-Q water to achieve a concentration of approximately 2×10^{-3} M. Cu^{2+} and Ag^+ stock solutions were prepared from analytical-grade salt ($CuCl_2$ or $AgNO_3$) and standardized using ICP-MS (10^{-3}–10^{-2} M). The ionic strength (I) was maintained at 0.15 M using sodium chloride (NaCl) or sodium nitrate ($NaNO_3$), as specified in each case. All experiments were performed in MilliQ water at least in triplicate to ensure reproducibility.

3.3.2. Formation kinetics. The complexation kinetics were qualitatively assessed at ambient temperature by recording the UV-Vis (Cu^{2+}) or ^{1}H-NMR (Ag^+) spectra of aqueous solutions containing the metal ion and DO2S2Py immediately after the mixing and over time. These solutions were prepared at a final concentration equal to 10^{-3} M for ^{1}H NMR and 10^{-3}–10^{-4} M for UV-Vis (1 : 1 metal-to-ligand ratio) in buffered media (*e.g.*, pH 2 HCl 10^{-2} M, pH 4.5 acetic/acetate buffer). To ensure the equilibrium was reached, the spectra of all samples were also re-acquired after heating at T = 80 °C until no further changes were observed.

3.3.3. Thermodynamic measurements

Potentiometry. Automatic pH-potentiometric titrations of DO2S2Py, Cu^{2+}-DO2S2Py, and Ag^+-DO2S2Py were carried out as described in detail in previous works.[38,40–42]

NMR. Variable-pH ^{1}H NMR spectra of DO2S2Py (~10^{-3} M) or Ag^+-DO2S2Py (~10^{-3} M, Ag^+ : L molar ratio of 1 : 1) were recorded at T = 25 °C in D_2O. The pH was adjusted by proper additions of DNO_3/DCl or CO_2-free NaOD. 0.41 log units were added to the instrumental pH values to account for isotopic effects, *i.e.* pD values instead of pH ones were considered.

UV-Vis. Variable-pH UV-Vis spectrophotometric titrations were conducted using the in-cell method for both the free DO2S2Py (C_L = 10^{-3}–10^{-2} M) and Cu^{2+}-DO2S2Py mixture (C_{Cu} = C_L = 10^{-3}–10^{-2} M, pH > 2) at T = 25 °C and I = 0.15 M NaCl. At pH < 2, the out-of-cell method was employed for Cu^{2+}-DO2S2Py, as described in our previous works.[40,41,55] Small volumes (~µL range) of HCl and/or NaOH were used to adjust the pH. The electronic spectra were recorded, and the equilibrium was reached when no further changes in either the pH or the electronic spectra were observed.

Data treatment. The protonation constants (pK_a) and overall equilibrium constants ($\log\beta$) were obtained by refinement of the thermodynamic data using different software (PITMAP, HypNMR, HyperSpec), as described in our previous publications.[41,55–57] Hydrolysis constants and solubility products of Cu^{2+} and Ag^+ in aqueous ionic media were taken from the literature.[58]

EPR measurements. EPR spectra were recorded with a BRUKER EleXsys E500 spectrometer using microwave frequency equal to 9.54 GHz, 13 mW microwave power, 5 G modulation amplitude and 100 kHz modulation frequency. Cu^{2+}-DO2S2Py aqueous solutions were prepared (10^{-3} M) and NaOH and HCl solutions were used to set the pH. The room temperature EPR spectra were recorded in capillaries (6 scans). For the frozen solution spectra, 0.2 mL samples were diluted with 0.05 mL of methanol to avoid crystallization of water and transferred into EPR tubes. Anisotropic EPR spectra were recorded in a dewar containing liquid nitrogen (77 K). The

Open Access Article. Published on 23 April 2026. Downloaded on 6/3/2026 9:25:06 AM. This article is licensed under a Creative Commons Attribution-NonCommercial 3.0 Unported Licence.

spectra were simulated by the "epr" program[59] using axial g-tensor ($g_\perp$, $g_\parallel$) and copper hyperfine tensor ($A_\perp^{Cu}$, $A_\parallel^{Cu}$) values. Orientation dependent linewidth parameters (α, β, γ) were used to fit the linewidths through the equation $\alpha_{M_I} = \alpha + \beta M_I + \gamma M_I^2$, where M_I denotes the magnetic quantum number of Cu^{2+}. Since a natural $CuCl_2$ was used for the measurements, the spectra were calculated by the summation of spectra of ^{63}Cu and ^{65}Cu weighted by their natural abundances. The room temperature spectra were simulated with the same software using the obtained anisotropic EPR parameters and fitting the rotational correlation times averaging the orientation dependence of the parameters.

3.4. Computational details

All the molecular geometry optimizations were performed by using the Gaussian16 package.[60] DFT level of theory was employed adopting the B3PW91 functional.[61] The 6-31G* basis set was chosen for all the atoms except for the Ag and Cu atoms for which the LANL2DZ pseudo-potential was employed together with the associated valence basis set.[62] A benchmark was carried out for selecting the most appropriate computational protocol able to reproduce the optical absorption spectra of the investigated systems simulated using time-dependent density functional theory (TDDFT) based on the optimized ground-state geometries. As a result of such benchmark for the Cu^{2+} complexes, the 6-31G* basis set adopted also for the Cu center was identified as the best performing one. Frequency calculations were performed at the same level of theory for all the optimized geometrical structures to confirm their nature of minima and for zero-point energy correction calculations. All calculations were carried out in water solvent (ε = 78.4), using Tomasi's implicit polarizable continuum model (PCM) as implemented in Gaussian16.[62–64]

For each complexation reaction, the free energy was computed replacing water molecules in the reference complexes. The reference complex for Cu^{2+} is square planar, with four water molecules in the first coordination sphere and two water molecules in the second coordination sphere. For Ag^+, the reference complex is linear, with two water molecules in the first coordination sphere.

The free energies of formation of these complexes are calculated using the reaction (1):

$$[M(H_2O)_n]^z + L \rightarrow [ML]^z + nH_2O \quad (1)$$

where L represents DO2S2Py, n corresponds to the number of coordinated water molecules in the reference complex (6 for Cu^{2+}, representing the hexa-aquo complex, and 2 for Ag^+, representing the bi-aquo complex), and z denotes the overall charge of the complex (+2 for Cu^{2+} and +1 for Ag^+).

Gibbs free energies were obtained at T = 25 °C and 1 atm including zero-point and thermal corrections. Therefore, the formation energies of the examined complexes were calculated as:

$$\Delta G = \Delta G([ML]^z) + n\Delta G(H_2O) - \Delta G([M(H_2O)_n]^z) - \Delta G(L) \quad (2)$$

The stability constant (logβ) value is related to free energy change for the complexation reaction by:

$$\log\beta = -\frac{\Delta G}{2.303RT} \quad (3)$$

Complexation energies were corrected for the basis set superposition error (BSSE) by using the Boys-Bernardi counterpoise technique.[65]

3.5. Kinetic inertness

3.5.1. Competition with metal ions. Competitive metal ions (Zn^{2+}, Mg^{2+}, Ca^{2+}, $n_{competitor}/n_{complex}$ = 10) or PBS (1 : 1 V/V dilution) were added to a solution of the preformed complexes and spectral variations induced by the additions of the competitor were monitored at room temperature over time using UV-Vis (Cu^{2+}; $C_{DO2S2Py} = C_{Cu} = 1 \times 10^{-4}$ M) or ^{1}H-NMR (Ag^+; $C_{DO2S2Py} = C_{Ag} = 1 \times 10^{-3}$ M). All experiments were performed in MilliQ water at least in triplicate to ensure reproducibility.

3.5.2. Acid-mediated decomplexation kinetics. Acid-mediated decomplexation studies of $[Cu(DO2S2Py)]^{2+}$ were performed under pseudo-first-order conditions in HCl at T = 25 °C, as described in our previous work.[40] The $^dk_{obs}$ values were calculated from the experimental data by using a single-exponential model $A(t) = A(0)\cdot e^{-k_{obs}\cdot t}$. The corresponding half-life was obtained from the equation $t_{1/2} = \ln 2/^dk_{obs}$.

3.6. Cyclic voltammetry

CV measurements were carried out in a conventional three-electrode cell equipped with a glassy carbon (GC, Metrohm) working electrode, a platinum wire counter electrode, and an Ag/AgCl (3 M KCl, Amel) reference electrode. Prior to each experiment, the GC electrode was polished with 0.05 μm alumina slurry and thoroughly rinsed with an ethanol/water mixture. Cyclic voltammograms were recorded at room temperature in aqueous 0.15 M $NaNO_3$ containing Cu^{2+} ($C_{DO2S2Py} = 8 \times 10^{-4}$ M) and ligand ($C_{Cu} = 8 \times 10^{-4}$ M) at pH 7.

3.7. Radiochemical experiments

Caution! ^{64}Cu and ^{111}Ag are radionuclides that emit ionizing radiation and were manipulated in a specifically designed facility under appropriate safety controls.

3.7.1. $[^{64}Cu]Cu^{2+}$. $[^{64}Cu]CuCl_2$ was obtained as previously described and appropriately diluted in 0.05 M HCl.[66] DO2S2Py and NOTA (reference) stock solutions were prepared in ultrapure metal-free water at 10^{-3} M and diluted appropriately to give a serial dilution series (10^{-4}–10^{-7} M). Radiolabeling was performed by mixing $[^{64}Cu]Cu^{2+}$ (1 MBq, 10 μL) to a solution containing the ligand (10 μL) diluted in an appropriate buffer (80 μL of either 0.1 M sodium acetate – final pH 4.5, or PBS 1× – final pH 7). A negative control (free $[^{64}Cu]Cu^{2+}$) was performed by substituting the ligand with an equal volume (10 μL) of H_2O. Different apparent molar activities were tested from 0.1 to 1000 MBq nmol^{-1}, corresponding to a final ligand concentration ranging from

 This journal is © the Partner Organisations 2026

Open Access Article. Published on 23 April 2026. Downloaded on 6/3/2026 9:25:06 AM. This article is licensed under a Creative Commons Attribution-NonCommercial 3.0 Unported Licence.

10^{-4} to 10^{-8} M. The reaction mixtures were allowed to react at ambient temperature or 95 °C and the radiochemical yields (RCY%) were monitored at different time points (5 min–1 h). All radiolabeling reactions were repeated at least in triplicate. RCY% was determined *via* radio-thin layer chromatography (radio-TLC) using iTLC-SA plates as stationary phase and EDTA (0.1 M, pH 5) as mobile phase. Under these conditions, free $[^{64}Cu]Cu^{2+}$ migrates with the solvent front (R_f = 1) while $[^{64}Cu]Cu^{2+}$ complexes remain at the baseline (R_f = 0). The iTLC plates were analyzed on an Eckert & Ziegler AR-2000 TLC scanner, and all the data were processed with Eckert & Ziegler WinScan software.

3.7.2. $[^{111}Ag]Ag^{+}$. ^{111}Ag was produced at the Institute Laue-Langevin (ILL, Grenoble, France) and purified at the Hevesy Laboratory (Denmark) using the anion exchange Dowex 1 × 8 and obtained in 6 M HCl. The fractions containing ^{111}Ag were evaporated and subsequently diluted in 1 M HCl.[43] DO2S2Py and DO4S (reference) stock solutions were prepared in ultrapure metal-free water at 10^{-3} M and diluted appropriately to give a serial dilution series (10^{-4}–10^{-7} M). Radiolabeling was executed by the addition of $[^{111}Ag]Ag^{+}$ (6.4 μL, 1 MBq) to a solution containing the ligand (10 μL) at the proper concentration diluted in phosphate buffer (50 mM, pH 7.4, 83.6 μL). A negative control (free $[^{111}Ag]Ag^{+}$) was performed by substituting the ligand with an equal volume of H_2O. Different apparent molar activities were tested from 0.1 to 1000 MBq nmol^{-1}, corresponding to a final ligand concentration ranging from 10^{-4} to 10^{-8} M. The radiolabeling reactions were conducted at RT or at T = 95 °C. All experiments were repeated in triplicate and monitored over time (5 min, 1 h) *via* radio-TLC using silica gel 60 F254 aluminum plates and $CHCl_3$: CH_3OH 9 : 1 + 0.1% NH_4OH as mobile phase. Under these conditions, free $[^{111}Ag]Ag^{+}$ is retained at the origin (R_f = 0) while $[^{111}Ag][Ag(DO2S2Py)]^{+}$ has R_f = 0.6. To track the radiolabeling of $[^{111}Ag][Ag(DO4S)]^{+}$, the conditions previously described were used.[43] The TLC plates were exposed to a multi-sensitive medium phosphor screen (PerkinElmer) and analyzed using a Cyclone Plus Storage Phosphor System (PerkinElmer).

3.7.3. *In vitro* stability assays. The integrity of $[^{64}Cu][Cu(DO2S2Py)]^{2+}$ and $[^{111}Ag][Ag(DO2S2Py)]^{+}$ was assessed in PBS and human serum by diluting the radiolabeled complexes (RCY > 99% prior to incubation) with an equal volume of PBS or human serum (1 : 1 V/V dilution), respectively. The 1 : 1 V/V dilution was selected to maintain consistency with previously conducted studies, allowing reliable comparison of the data. The solutions were incubated at T = 37 °C to simulate the biological environment. The integrity of the radiometal complexes was monitored over time *via* radio-TLC, using the mobile and stationary phases described above. Free $[^{64}Cu]Cu^{2+}$ and free $[^{111}Ag]Ag^{+}$ in human serum were used as controls. Any $[^{64}Cu]Cu^{2+}$ transchelated with serum proteins migrated with EDTA solvent front ($R_f \sim 1$), while intact radiometal complex remained at the baseline ($R_f \sim 0$). In contrast, any $[^{111}Ag]Ag^{+}$ transchelated with serum proteins remained at the baseline ($R_f \sim 0$) while intact metal complex had R_f = 0.6. The percentage of intact complex was determined by integrating the areas under the curves corresponding to the free and intact species.

4. Conclusions

Coinage radiometals such as $^{103/111}Ag$ and $^{64/67}Cu$ offer significant opportunities for cancer theranostics by providing matched diagnostic and therapeutic radionuclides within the same chemical family. Their successful *in vivo* application, however, critically depends on chelators capable of maintaining stable metal coordination *in vivo*. Despite their promise, the clinical translation of $^{103/111}Ag$ remains severely limited by the lack of robust chelating systems, while redox-induced decomplexation continues to challenge the stability of $^{64/67}Cu$-based radiopharmaceuticals. In this context, the development of a single ligand platform capable of efficiently coordinating both silver and copper represents a significant breakthrough that would enable the preparation of chemically analogous radiopharmaceuticals that differ only in radionuclide identity.

Building on our previous work on sulfur-containing macrocycles for the chelation of theranostic radiometals, we sought to enhance the biological stability of the resulting radiometal complexes. Although these earlier ligands displayed promising coordination properties, the corresponding radioactive complexes showed only moderate stability under biologically relevant conditions. To address this limitation, we incorporated pyridine donor units in the macrocyclic framework, creating a sterically protected coordination environment.

The resulting ligand, DO2S2Py, rapidly coordinates both Cu^{2+} and Ag^{+}, forming complexes that are highly thermodynamically stable and kinetically inert. In $[Cu(DO2S2Py)]^{2+}$, the copper center adopts a distorted elongated octahedral geometry involving the two pyridine nitrogen atoms and the four nitrogens from the cyclen backbone ($4N_{cy}2N_{py}$). In contrast, $[Ag(DO2S2Py)]^{+}$ displays multiple coordination modes in aqueous solutions ($4N_{cy}1N_{py}1S$ and $4N_{cy}2N_{py}$) reflecting the adaptable yet strongly binding nature of the ligand scaffold. In both cases, the pyridine donors play a key role in reinforcing metal coordination and enhancing complex stability.

Importantly, DO2S2Py also efficiently complexes the corresponding radioactive isotopes (^{64}Cu and ^{111}Ag) under highly diluted radiochemical conditions and mild labeling protocols. $[^{64}Cu][Cu(DO2S2Py)]^{2+}$ exhibited exceptional stability in biologically relevant media (>95% intact after 24 h), specifically PBS and human serum. Although $[^{111}Ag][Ag(DO2S2Py)]^{+}$ was less stable (75% intact after 24 h in human serum), it showed improved performance compared to the current best-performing chelator for ^{111}Ag, *i.e.* DO4S.

Collectively, these results demonstrate that incorporation of pyridine donors effectively enhances complex stability and inertness in biological environments, thereby validating our design strategy. Overall, DO2S2Py represents a significant step toward the development of a unified chelator platform capable

Open Access Article. Published on 23 April 2026. Downloaded on 6/3/2026 9:25:06 AM. This article is licensed under a Creative Commons Attribution-NonCommercial 3.0 Unported Licence.

of stabilizing theranostic coinage radiometals under physiologically relevant conditions.

Author contributions

The manuscript was written through contributions of all authors. All authors have given approval to the final version of the manuscript. M. T.: conceptualization, data curation, formal analysis, investigation, methodology, project administration, writing – original draft; F. P.: investigation, methodology, writing – review & editing; S. F.: methodology, writing – review & editing; N. V. M.: investigation, methodology, writing – review & editing; M. J.: funding acquisition, supervision, resources, writing – review & editing; H. M.: funding acquisition, supervision, writing – review & editing; V. D. M.: supervision, writing – review & editing; L. P.: supervision, resources, writing – review & editing; E. F.: funding acquisition, supervision, resources, writing – review & editing; E. S.: funding acquisition, supervision, resources, writing – review & editing; M. A.: funding acquisition, supervision, writing – review & editing; C. F.: funding acquisition, supervision, resources, writing – review & editing.

Conflicts of interest

The authors have no competing interests to declare.

Data availability

The authors confirm that the data supporting the findings of this study are available within the article and its supplementary information (SI). Supplementary information: NMR and MS characterization of di-Boc-cyclen, di-Boc-DO2S, DO2S, and DO2S2Py; pH-dependent UV-Vis titrations of DO2S2Py and corresponding speciation plots; UV-Vis studies of Cu^{2+}-DO2S2Py (formation kinetics and thermodynamics); NMR characterization of Ag^{+}-DO2S2Py (formation kinetics and thermodynamics); ESI-MS analysis of Cu^{2+}-DO2S2Py; comparison of pCu^{2+} values with related py-containing chelators; EPR spectra of $[Cu(DO2S2Py)]^{2+}$; DFT data for Cu^{2+}-DO2S2Py, Ag^{+}-DO2S2Py, and Cu^{+}-DO2S2Py; kinetic studies in the presence of competing metal ions and PBS; acid-assisted decomplexation kinetics; cyclic voltammogram of $[Cu(DO2S2Py)]^{2+}$; radiochemistry studies with ^{64}Cu and ^{111}Ag and comparison with reference chelators (NOTA and DO4S). See DOI: **https://doi.org/10.1039/d6qi00525j**.

Acknowledgements

This research was supported by the European Union's Horizon 2020 research and innovation program as a user project of PRISMAP – The European medical radionuclides program (GA 101008571) and the New Frontiers in Research Fund Transformation Program "Rare Isotopes to Transform Cancer Therapy" (NFRFT-2022-00269). TRIUMF receives funding from a contribution agreement with the National Research Council of Canada. The work was also partly supported by the Italian Ministry of Health – Ricerca Corrente Annual Program 2025, AUSL-IRCCS Reggio Emilia (Italy). The authors gratefully acknowledge Prof. Ulli Köster and ILL (Grenoble, France) for performing irradiations of ^{110}Pd targets for PRISMAP. The authors would like to thank the "Centro Interdipartimentale Grandi Strumenti C.I.G.S." of the University of Modena and Reggio Emilia (**https://www.cigs.unimore.it**, Modena, Italy) for NMR, mass spectrometers and their technical support.

References

1 M. Tosato and M. Asti, Lights and Shadows on the Sourcing of Silver Radioisotopes for Targeted Imaging and Therapy of Cancer: Production Routes and Separation Methods, *Pharmaceuticals*, 2023, **16**, 929.
2 K. A. Morgan, S. E. Rudd, A. Noor and P. S. Donnelly, Theranostic Nuclear Medicine with Gallium-68, Lutetium-177, Copper-64/67, Actinium-225, and Lead-212/203 Radionuclides, *Chem. Rev.*, 2023, **123**, 12004–12035.
3 N. Yang, X. Guo, J. Ding, F. Wang, T. Liu, H. Zhu and Z. Yang, Copper-64 Based PET-Radiopharmaceuticals: Ways to Clinical Translational, *Semin. Nucl. Med.*, 2024, **54**, 792–800.
4 *Copper-64 Radiopharmaceuticals: Production, Quality Control and Clinical Applications*, International Atomic Energy Agency, Vienna, 2022.
5 **https://www-nds.iaea.org/relnsd/vcharthtml/VChartHTML.html** (accessed April 20 2026).
6 O. O. Krasnovskaya, D. Abramchuck, A. Erofeev, P. Gorelkin, A. Kuznetsov, A. Shemukhin and E. K. Beloglazkina, Recent Advances in $^{64}Cu/^{67}Cu$-Based Radiopharmaceuticals, *Int. J. Mol. Sci.*, 2023, **24**, 9154.
7 P. Kręcisz, K. Stefańska, J. Studziński, M. Pitucha, A. Czylkowska and P. Szymański, Radiocopper in Radiopharmacy and Medical Use: Current Status and Perspective, *J. Med. Chem.*, 2025, **68**, 2356–2376.
8 E. Boros and A. B. Packard, Radioactive Transition Metals for Imaging and Therapy, *Chem. Rev.*, 2019, **119**, 870–901.
9 M. Shokeen and C. J. Anderson, Coordination Chemistry of Bifunctional Chemical Agents Designed for Applications in ^{64}Cu PET Imaging for Alzheimer's Disease, *Acc. Chem. Res.*, 2009, **42**, 832–841.
10 P. J. Blower, J. S. Lewis and J. Zweit, Copper Radionuclides and Radiopharmaceuticals in Nuclear Medicine, *Nucl. Med. Biol.*, 1996, **23**, 957–980.
11 T. Mastren, V. Radchenko, J. W. Engle, J. W. Weidner, A. Owens, L. E. Wyant, R. Copping, M. Brugh, F. M. Nortier, E. R. Birnbaum, K. D. John and M. E. Fassbender, Chromatographic Separation of the Theranostic Radionuclide ^{111}Ag From a Proton Irradiated Thorium Matrix, *Anal. Chim. Acta*, 2018, **998**, 75–82.

 This journal is © the Partner Organisations 2026

Open Access Article. Published on 23 April 2026. Downloaded on 6/3/2026 9:25:06 AM. This article is licensed under a Creative Commons Attribution-NonCommercial 3.0 Unported Licence.

12 M. Tosato, A. Gandini, S. Happel, M. Bas, A. Donzella, A. Zenoni, A. Salvini, A. Andrighetto, V. Di Marco and M. Asti, Chromatographic Separation of Silver-111 from Neutron-irradiated Palladium Target: Toward Direct Labeling of Radiotracers, *EJNMMI Radiopharm. Chem.*, 2023, **8**, 43.

13 T. A. Aweda, O. Ikotun, T. Mastren, C. L. Cannon, B. Wright, W. J. Youngs, C. Cutler, J. Guthrie and S. E. Lapi, The Use of ^{111}Ag as a Tool for Studying Biological Distribution of Silver-Based Antimicrobials, *Med. Chem. Commun.*, 2013, **4**, 1015–1017.

14 S. Chattopadhyay, K. V. Vimalnath, S. Saha, A. Korde, H. D. Sarma, S. Pal and M. K. Das, Preparation and Evaluation of a New Radiopharmaceutical for Radiosynovectomy, ^{111}Ag-labelled Hydroxyapatite (HA) Particles, *Appl. Radiat. Isot.*, 2008, **66**, 334–339.

15 N. Ukon, M. Aikawa, Y. Komori and H. Haba, Production Cross Sections of Deuteron-Induced Reactions on Natural Palladium for Ag Isotopes, *Nucl. Instrum. Methods Phys. Res., Sect. B*, 2018, **426**, 13–17.

16 E. W. Price and C. Orvig, Matching Chelators to Radiometals for Radiopharmaceuticals, *Chem. Soc. Rev.*, 2014, **43**, 260–290.

17 N. C. Okoye, J. E. Baumeister, F. N. Khosroshahi, H. M. Hennkens and S. S. Jurisson, Chelators and Metal Complex Stability for Radiopharmaceutical Applications, *Radiochim. Acta*, 2019, **107**, 1087–1120.

18 E. Boros, B. V. Marquez, O. F. Ikotun, S. E. Lapi and C. L. Ferreira, Coordination Chemistry and Ligand Design in the Development of Metal Based Radiopharmaceuticals, in *Ligand Design in Medicinal Inorganic Chemistry*, John Wiley & Sons, Ltd, 2014, pp. 47–79.

19 D. Sneddon and B. Cornelissen, Emerging Chelators for Nuclear Imaging, *Curr. Opin. Chem. Biol.*, 2021, **63**, 152–162.

20 T. I. Kostelnik and C. Orvig, Radioactive Main Group and Rare Earth Metals for Imaging and Therapy, *Chem. Rev.*, 2019, **119**, 902–956.

21 C. S. Cutler, H. M. Hennkens, N. Sisay, S. Huclier-Markai and S. S. Jurisson, Radiometals for Combined Imaging and Therapy, *Chem. Rev.*, 2013, **113**, 858–883.

22 K. S. Woodin, K. J. Heroux, C. A. Boswell, E. H. Wong, G. R. Weisman, W. Niu, S. A. Tomellini, C. J. Anderson, L. N. Zakharov and A. L. Rheingold, Kinetic Inertness and Electrochemical Behavior of Copper(II) Tetraazamacrocyclic Complexes: Possible Implications for in Vivo Stability, *Eur. J. Inorg. Chem.*, 2005, **2005**, 4829–4833.

23 M. S. Cooper, M. T. Ma, K. Sunassee, K. P. Shaw, J. D. Williams, R. L. Paul, P. S. Donnelly and P. J. Blower, Comparison of ^{64}Cu-complexing Bifunctional Chelators for Radioimmunoconjugation: Labeling Efficiency, Specific Activity, and *In Vitro*/*In Vivo* Stability, *Bioconjugate Chem.*, 2012, **23**, 1029–1039.

24 L. A. Bass, M. Wang, M. J. Welch and C. J. Anderson, *In Vivo* Transchelation of Copper-64 from TETA-Octreotide to Superoxide Dismutase in Rat Liver, *Bioconjugate Chem.*, 2000, **11**, 527–532.

25 C. F. Ramogida, E. Boros, B. O. Patrick, S. K. Zeisler, J. Kumlin, M. J. Adam, P. Schaffer and C. Orvig, Evaluation of H_2CHXdedpa, H_2dedpa- and H_2CHXdedpa-N,N′-propyl-2-NI ligands for ^{64}Cu(II) Radiopharmaceuticals, *Dalton Trans.*, 2016, **45**, 13082–13090.

26 M. Le Fur, M. Beyler, N. Le Poul, L. M. P. Lima, Y. Le Mest, R. Delgado, C. Platas-Iglesias, V. Patinec and R. Tripier, Improving the Stability and Inertness of Cu(II) and Cu(I) Complexes with Methylthiazolyl Ligands by Tuning the Macrocyclic Structure, *Dalton Trans.*, 2016, **45**, 7406–7420.

27 S. N. Rylova, C. Stoykow, L. Del Pozzo, K. Abiraj, M. L. Tamma, Y. Kiefer, M. Fani and H. R. Mäcke, The Somatostatin Receptor 2 Antagonist ^{64}Cu-NODAGA-JR11 Outperforms ^{64}Cu-DOTA-TATE in a Mouse Xenograft Model, *PLoS One*, 2018, **13**, 1–16.

28 T. J. Wadas, E. H. Wong, G. R. Weisman and C. J. Anderson, Coordinating Radiometals of Copper, Gallium, Indium, Yttrium, and Zirconium for PET and SPECT Imaging of Disease, *Chem. Rev.*, 2010, **110**, 2858–2902.

29 S. V. Smith, Molecular Imaging with Copper-64, *J. Inorg. Biochem.*, 2004, **98**, 1874–1901.

30 C. A. Boswell, X. Sun, W. Niu, G. R. Weisman, E. H. Wong, A. L. Rheingold and C. J. Anderson, Comparative *In Vivo* Stability of Copper-64-labeled Cross-bridged and Conventional Tetraazamacrocyclic Complexes, *J. Med. Chem.*, 2004, **47**, 1465–1474.

31 E. H. Wong, G. R. Weisman, D. C. Hill, D. P. Reed, M. E. Rogers, J. S. Condon, M. A. Fagan, J. C. Calabrese, K.-C. Lam, I. A. Guzei and A. L. Rheingold, Synthesis of a Cross-Bridged Cyclam Derivative for Peptide Conjugation and ^{64}Cu Radiolabeling, *J. Am. Chem. Soc.*, 2000, **122**, 10561–10572.

32 R. Ferdani, D. J. Stigers, A. L. Fiamengo, L. Wei, B. T. Y. Li, J. A. Golen, A. L. Rheingold, G. R. Weisman, E. H. Wong and C. J. Anderson, Synthesis, Cu(II) Complexation, 64Cu-labeling and Biological Evaluation of Cross-bridged Cyclam Chelators with Phosphonate Pendant Arms, *Dalton Trans.*, 2012, **41**, 1938–1950.

33 R. G. Pearson, Hard and Soft Acids and Bases, HSAB, Part 1: Fundamental Principles, *J. Chem. Educ.*, 1968, **45**, 581.

34 A. Donzella, A. Leso, A. Arzenton, G. Bonomi, S. Bortolussi, D. Chen, S. Corradetti, M. Lunardon, E. Mariotti, E. Reniero, D. Serafini, G. S. Valli, L. Zangrando, A. Zenoni and A. Andrighetto, Monte Carlo Dosimetry of Silver-111 in Simplified Cell Geometries in the Framework of the ISOLPHARM Project, *Appl. Radiat. Isot.*, 2025, **225**, 111979.

35 L. Morselli, A. Donzella, A. Arzenton, M. Asti, S. Bortolussi, S. Corradetti, G. D'Agostino, M. D. Luzio, M. Ferrari, A. Gandini, M. Lunardon, V. Villa, A. Salvini, L. Zangrando, A. Zenoni and A. Andrighetto, Production and Characterization of ^{111}Ag Radioisotope for Medical Use in A TRIGA Mark II Nuclear Research Reactor, *Appl. Radiat. Isot.*, 2023, **197**, 110798.

36 K. M. El-Azony, N. M. A. Mohamed and D. A. Aloraini, Advantages and Disadvantages of Nuclear Reactions Used

Open Access Article. Published on 23 April 2026. Downloaded on 6/3/2026 9:25:06 AM. This article is licensed under a Creative Commons Attribution-NonCommercial 3.0 Unported Licence.

in Reactors or Cyclotrons, in Addition to a Theoretical Study Based on Photodisintegration on Natural Indium for ^{111}Ag Production, *Nucl. Sci. Tech.*, 2022, **33**, 14.

37 M. Ballan, M. Tosato, M. Verona, M. Caeran, F. Borgna, E. Vettorato, S. Corradetti, L. Zangrando, M. Sgaravatto, M. Verlato, M. Asti, G. Marzaro, F. Mastrotto, V. Di Marco, D. Maniglio, A. Bisio, A. Motta, A. Quaranta, A. Zenoni, P. Pastore, N. Realdon and A. Andrighetto, Preliminary Evaluation of the Production of Non-Carrier Added ^{111}Ag as Core of a Therapeutic Radiopharmaceutical in the Framework of ISOLPHARM_Ag Experiment, *Appl. Radiat. Isot.*, 2020, **164**, 109258.

38 M. Tosato, M. Dalla Tiezza, N. V. May, A. A. Isse, S. Nardella, L. Orian, M. Verona, C. Vaccarin, A. Alker, H. Mäcke, P. Pastore and V. Di Marco, Copper Coordination Chemistry of Sulfur Pendant Cyclen Derivatives: An Attempt to Hinder the Reductive-Induced Demetalation in $^{64/67}$Cu Radiopharmaceuticals, *Inorg. Chem.*, 2021, **60**, 11530–11547.

39 M. Tosato, M. Verona, C. Favaretto, M. Pometti, G. Zanoni, F. Scopelliti, F. P. Cammarata, L. Morselli, Z. Talip, N. P. van der Meulen, V. Di Marco and M. Asti, Chelation of Theranostic Copper Radioisotopes with S-Rich Macrocycles: From Radiolabelling of Copper-64 to In Vivo Investigation, *Molecules*, 2022, **27**(13), 4158.

40 M. Tosato, M. Pelosato, S. Franchi, A. A. Isse, N. V. May, G. Zanoni, F. Mancin, P. Pastore, D. Badocco, M. Asti and V. Di Marco, When Ring Makes the Difference: Coordination Properties of Cu^{2+}/Cu^{+} Complexes with Sulfur-Pendant Polyazamacrocycles for Radiopharmaceutical Applications, *New J. Chem.*, 2022, **46**, 10012–10025.

41 M. Tosato, S. Franchi, A. A. Isse, A. Del Vecchio, G. Zanoni, A. Alker, M. Asti, T. Gyr, V. Di Marco and H. Mäcke, Is Smaller Better? Cu^{2+}/Cu^{+} Coordination Chemistry and Copper-64 Radiochemical Investigation of a 1,4,7-Triazacyclononane-Based Sulfur-Rich Chelator, *Inorg. Chem.*, 2023, **62**, 20621–20633.

42 M. Tosato, M. Asti, M. Dalla Tiezza, L. Orian, D. Häussinger, R. Vogel, U. Köster, M. Jensen, A. Andrighetto, P. Pastore and V. Di Marco, Highly Stable Silver(I) Complexes with Cyclen-Based Ligands Bearing Sulfide Arms: A Step Toward Silver-111 Labeled Radiopharmaceuticals, *Inorg. Chem.*, 2020, **59**, 10907–10919.

43 M. Tosato, S. Franchi, M. Dalla Tiezza, L. Orian, T. Gyr, A. Alker, G. Zanoni, P. Pastore, A. Andrighetto, U. Köster, M. Jensen, H. Mäcke, M. Asti and V. Di Marco, Tuning the Framework of Thioether-Functionalized Polyazamacrocycles: Searching for a Chelator for Theranostic Silver Radioisotopes, *Inorg. Chem.*, 2023, **62**, 20777–20790.

44 M. Tosato, M. Asti, V. Di Marco, M. L. Jensen, J. Schell, T. T. Dang, U. Köster, M. Jensen and L. Hemmingsen, Towards In Vivo Applications of ^{111}Ag Perturbed Angular Correlation of γ-Rays (PAC) Spectroscopy, *Appl. Radiat. Isot.*, 2022, **190**, 110508.

45 M. Tosato, P. Randhawa, L. Lazzari, B. L. McNeil, M. Dalla Tiezza, G. Zanoni, F. Mancin, L. Orian, C. F. Ramogida and V. Di Marco, Tuning the Softness of the Pendant Arms and the Polyazamacrocyclic Backbone to Chelate the ^{203}Pb/^{212}Pb Theranostic Pair, *Inorg. Chem.*, 2024, **63**, 1745–1758.

46 M. Tosato, P. Randhawa, M. Asti, L. B. S. Hemmingsen, C. A. O'Shea, P. Thaveenrasingam, S. P. A. Sauer, S. Chen, C. Graiff, I. Menegazzo, M. Baron, V. Radchenko, C. F. Ramogida and V. Di Marco, Capturing Mercury-197 m/g for Auger Electron Therapy and Cancer Theranostic with Sulfur-Containing Cyclen-Based Macrocycles, *Inorg. Chem.*, 2024, **63**, 14241–14255.

47 M. Tosato, M. Verona, R. Doro, M. Dalla Tiezza, L. Orian, A. Andrighetto, P. Pastore, G. Marzaro and V. Di Marco, Toward Novel Sulphur-Containing Derivatives of Tetraazacyclododecane: Synthesis, Acid–Base Properties, Spectroscopic Characterization, DFT Calculations, and Cadmium(II) Complex Formation in Aqueous Solution, *New J. Chem.*, 2020, **44**, 8337–8350.

48 M. Trose, M. Dell'Acqua, T. Pedrazzini, V. Pirovano, E. Gallo, E. Rossi, A. Caselli and G. Abbiati, [Silver(I) (Pyridine-Containing Ligand)] Complexes As Unusual Catalysts for A3-Coupling Reactions, *J. Org. Chem.*, 2014, **79**, 7311–7320.

49 H. Tsukube, S. Shinoda, J. Uenishi, T. Hiraoka, T. Imakoga and O. Yonemitsu, Ag^{+}-Specific Pyridine Podands: Effects of Ligand Geometry and Stereochemically Controlled Substitution on Cation Complexation and Transport Functions, *J. Org. Chem.*, 1998, **63**, 3884–3894.

50 S. El Ghachtouli, C. Cadiou, I. Déchamps-Olivier, F. Chuburu, M. Aplincourt and T. Roisnel, (Cyclen– and cyclam–pyridine)copper Complexes: The Role of the Pyridine Moiety in Cu^{II} and Cu^{I} Stabilisation, *Eur. J. Inorg. Chem.*, 2006, **2006**, 3472–3481.

51 N. Bernier, J. Costa, R. Delgado, V. Félix, G. Royal and R. Tripier, Monopicolinate Cyclen and Cyclam Derivatives for Stable Copper(II) Complexation, *Dalton Trans.*, 2011, **40**, 4514–4526.

52 A. Bianchi, M. Micheloni and P. Paoletti, Thermodynamic Aspects of the Polyazacycloalkane Complexes with Cations and Anions, *Coord. Chem. Rev.*, 1991, **110**, 17–113.

53 E. Boros, P. Comba, J. W. Engle, C. Harriswangler, S. E. Lapi, J. S. Lewis, S. Mastroianni, L. M. Mirica, C. Platas-Iglesias, C. F. Ramogida, R. Tripier and M. Tosato, Chemical Tools to Characterize the Coordination Chemistry of Radionuclides for Radiopharmaceutical Applications, *Chem. Rev.*, 2025, **125**, 12030–12068.

54 T. A. Kaden, Model Complexes for Biologically Active Copper, *Port. Electrochim. Acta*, 1993, **10**, 109–120.

55 M. Tosato, M. Boniburini, F. Faglioni, F. Genua, M. Mari, J. Storchi, S. Franchi, M. Asti and E. Ferrari, Thwarting Isomerization through Rigidity: A Promising HBED

 This journal is © the Partner Organisations 2026

Open Access Article. Published on 23 April 2026. Downloaded on 6/3/2026 9:25:06 AM.
This article is licensed under a Creative Commons Attribution-NonCommercial 3.0 Unported Licence.

Derivative for the Chelation of Gallium-68, *Inorg. Chem.*, 2025, **64**, 18673–18686.
56 V. Di Marco, PhD Thesis, University of Padova, 1998.
57 **https://www.hyperquad.co.uk/** (accessed April 20 2026).
58 C. F. J. Baes and R. E. Mesmer, *The Hydrolysis of Cations*, Wiley-Interscience, New York, 1976.
59 A. Rockenbauer and L. Korecz, Automatic Computer Simulations of ESR Spectra, *Appl. Magn. Reson.*, 1996, **10**, 29–43.
60 M. J. Frisch, G. W. Trucks, H. B. Schlegel, G. E. Scuseria, M. A. Robb, J. R. Cheeseman, G. Scalmani, V. Barone, G. A. Petersson, H. Nakatsuji, X. Li, M. Caricato, A. V. Marenich, J. Bloino, B. G. Janesko, R. Gomperts, B. Mennucci, H. P. Hratchian, J. V. Ortiz, A. F. Izmaylov, J. L. Sonnenberg, D. Williams-Young, F. Ding, F. Lipparini, F. Egidi, J. Goings, B. Peng, A. Petrone, T. Henderson, D. Ranasinghe, V. G. Zakrzewski, J. Gao, N. Rega, G. Zheng, W. Liang, M. Hada, M. Ehara, K. Toyota, R. Fukuda, J. Hasegawa, M. Ishida, T. Nakajima, Y. Honda, O. Kitao, H. Nakai, T. Vreven, K. Throssell, J. A. Montgomery Jr., J. E. Peralta, F. Ogliaro, M. J. Bearpark, J. J. Heyd, E. N. Brothers, K. N. Kudin, V. N. Staroverov, T. A. Keith, R. Kobayashi, J. Normand, K. Raghavachari, A. P. Rendell, J. C. Burant, S. S. Iyengar, J. Tomasi, M. Cossi, J. M. Millam, M. Klene, C. Adamo, R. Cammi, J. W. Ochterski, R. L. Martin, K. Morokuma, O. Farkas, J. B. Foresman and D. J. Fox, *Gaussian 16, Revision B.01*, Gaussian, Inc., Wallingford CT, 2016, GaussView 5.0. Wallingford, E.U.A.
61 A. D. Becke, Density–functional Thermochemistry. III. The Role of Exact Exchange, *J. Chem. Phys.*, 1993, **98**, 5648–5652.
62 P. J. Hay and W. R. Wadt, Ab Initio Effective Core Potentials for Molecular Calculations. Potentials for K to Au Including the Outermost Core Orbitals, *J. Chem. Phys.*, 1985, **82**, 299–310.
63 E. Cancès, B. Mennucci and J. Tomasi, A New Integral Equation Formalism for the Polarizable Continuum Model: Theoretical Background and Applications to Isotropic and Anisotropic Dielectrics, *J. Chem. Phys.*, 1997, **107**, 3032–3041.
64 B. Mennucci and J. Tomasi, Continuum Solvation Models: A New Approach to the Problem of Solute's Charge Distribution and Cavity Boundaries, *J. Chem. Phys.*, 1997, **106**, 5151–5158.
65 S. F. Boys and F. Bernardi, The Calculation of Small Molecular Interactions by the Differences of Separate Total Energies. Some Procedures with Reduced Errors, *Mol. Phys.*, 1970, **19**, 553–566.
66 H. Yang, F. Gao, B. McNeil, C. Zhang, Z. Yuan, S. Zeisler, J. Kumlin, J. Zeisler, F. Bénard, C. Ramogida and P. Schaffer, Synthesis of DOTA-pyridine Chelates for ^{64}Cu Coordination and Radiolabeling of αMSH Peptide, *EJNMMI Radiopharm. Chem.*, 2021, **6**, 3.